NREL/TP-411-7350 • UC Category: 1280 • DE95000245

Large-Area Triple-Junction a-Si Alloy Production Scaleup

Annual Subcontract Report 17 March 1993 – 18 March 1994

R. Oswald, J. Morris
Solarex Thin Film Division
Newtown, Pennsylvania

NREL technical monitor: R. Mitchell

National Renewable Energy Laboratory
1617 Cole Boulevard
Golden, Colorado 80401-3393
A national laboratory of the U.S. Department of Energy
Managed by Midwest Research Institute
for the U.S. Department of Energy
under contract No. DE-AC36-83CH10093

Prepared under Subcontract No. ZM-2-11040-2

November 1994

NOTICE

Available to DOE and DOE contractors from:
Office of Scientific and Technical Information (OSTI)
P.O. Box 62
Oak Ridge, TN 37831
Prices available by calling (615) 576-8401

Available to the public from:
National Technical Information Service (NTIS)
U.S. Department of Commerce
5285 Port Royal Road
Springfield, VA 22161
(703) 487-4650

Printed on paper containing at least 50% wastepaper and 10% postconsumer waste

DISCLAIMER

Portions of this document may be illegible electronic image products. Images are produced from the best available original document.

EXECUTIVE SUMMARY

Objectives: The objective of this subcontract over its three-year duration is to advance Solarex's photovoltaic manufacturing technologies, reduce its a-Si:H module production costs, increase module performance and expand the Solarex commercial production capacity. Solarex shall meet these objectives by improving the deposition and quality of the transparent front contact, by optimizing the laser patterning process, scaling-up the semiconductor deposition process, improving the back contact deposition, scaling-up and improving the encapsulation and testing of its a-Si:H modules. In the Phase II portion of this subcontract, Solarex focused on improving deposition of the front contact, investigating alternate feed stocks for the front contact, maximizing throughput and area utilization for all laser scribes, optimizing a-Si:H deposition equipment to achieve uniform deposition over large-areas, optimizing the triple-junction module fabrication process, evaluating the materials to deposit the rear contact, and optimizing the combination of isolation scribe and encapsulant to pass the wet high potential test.

Task 8: Front Contact Development

Optimization of our large-area front contact deposition process resulted in tin oxide films with resistivities as low as 3.6×10^{-4} ohm-cm. A prototype injector has been tested and modifications to this injector resulted in improved uniformity. Efforts to further improve the uniformity are ongoing. We have identified a dopant gas that is both safer and less expensive to use. This material is now our standard dopant material on our large-area furnace. In addition to alternative dopant materials, we have identified a promising alternative to our standard tin feed stock for tin oxide film deposition.

Task 9: Laser Scribe Process Development

Upgrades to the large-area laser scribe system and optimization of scribe parameters were essential to attaining laser scribe processes capable of throughput rates of 30 plates per hour with an area utilization of over 94%. Laser scribe rates of 0.3716 m^2 per minute (4 ft^2 per minute) on 0.557 m^2 (6 ft^2) substrates have been demonstrated for all four of the scribing processes. Total scribe widths of less than 676 μm (0.0266 in) have been attained at this high throughput rate.

Task 10: Amorphous Silicon Based Semiconductor Deposition

Upgrades to our large-area deposition system have resulted in a film thickness uniformity of ± 3.1% over a 0.74 m^2 substrate area. These upgrades included lower cost and thermally stable internal reactor parts, a six-zone substrate heater assembly, and multi-port gas injection and pumping system. Initial aperture-area conversion efficiencies of 10.3% on 0.1 m^2 and 8.12% on 0.37 m^2 substrates have been achieved.

Task 11: Rear Contact Deposition Process

Two sputter deposition processes for depositing zinc oxide films on large-areas have been developed. The first process uses a zinc oxide/aluminum oxide target in the radio frequency sputtering mode; the second process uses a zinc/aluminum target in the dc magnetron sputtering mode to reactively sputter deposit zinc oxide films. Both processes have been used to deposit highly reflecting zinc oxide/aluminum rear contacts over large-areas. The deposition rates for the dc reactive sputtering process have been found to be a factor of 4 higher than the deposition rates from the rf process.

Task 12: Frit/Bus/Wire/Frame

Development of a low-cost, environmentally reliable connector for large area modules has been completed. Work to develop alternative buss formulations is continuing and we have identified several equipment upgrades that promise to provide better control of the dispensing process over large-areas. Two classes of encapsulant materials that enable us to pass high potential tests have been identified. The utility of insulating films in combination with these encapsulant materials is now under investigation.

Task 13: Materials Handling

The compatibility of glass handling equipment with module processing equipment has been examined. Equipment layouts for the module fabrication line have been developed, as have layouts for raw material storage and finished goods inventory. Methods of inventory control for raw materials and finished goods have also been examined. Several pieces of packaging automation equipment have been identified.

Task 14: Environmental Test, Yield and Performance Analysis

An automated curing station to burn-out electrical shorts in triple-junction large-area modules has been designed and constructed. Debugging of this cure system is complete and the utility of this system in curing electrical shorts has been established. A comprehensive outdoor exposure study to evaluate the effect of module fabrication and environmental factors on module reliability has been completed. The cumulative yield of large-area modules, including high potential test yield was estimated to be 49.3%.

TABLE OF CONTENTS

TABLE OF CONTENTS CONTINUED

LIST OF FIGURES

LIST OF FIGURES CONTINUED

LIST OF TABLES

1.0 INTRODUCTION

Manufacturing large-area multi-junction devices at low cost requires that all component processes be thoroughly investigated for potential cost reductions, durability and capability. Transfer of multi-junction deposition processes from small single or multi-chamber systems to larger reactors requires total re-optimization of recipes and increased attention to deposition uniformity. The repeatability of laser processes must be maintained with the same precision over longer distances often at higher cutting speeds. Chemical vapor deposition (CVD) processes require new injector designs to maintain lateral uniformity of electrical and optical properties. New back contact materials deposited with reactive sputtering techniques need to maintain uniformity to insure reliable laser scribing. Encapsulants must be thoroughly tested environmentally and help provide for safe handling of high voltage interconnected panels. Many of these items have not been addressed in the research efforts to provide high efficiency stable amorphous silicon-alloy devices. Simultaneously, the processes all need to be scaled-up to handle larger size modules if cost efficiency goals are to be achieved.

2.0 TASK 8: FRONT CONTACT DEVELOPMENT

2.1 Introduction

During this phase, the effort has been focused on continued improvement of our front contact capability and performance. A multiple injector atmospheric pressure chemical vapor deposition (APCVD) furnace has been designed, built and tested for use in depositing tin oxide on substrates $\geq$ 0.56 m^2 (6 ft^2). The development work on an injector for this system has also continued as part of the process scale-up. In addition, process work has continued on the tin oxide coatings, and also alternate materials for making transparent conductive oxides.

2.2 Multiple Injector Tin Oxide System

To provide conductive tin oxide substrates at a low cost for multi-junction modules, it is necessary to develop a multiple injector APCVD tin oxide furnace. During this phase, an APCVD system capable of depositing both SiO_2 and SnO_2 films was fabricated and tested.

The system was designed to handle a nominal 1 MW per year worth of production capacity which is expandable to approximately 10 MW per year through equipment upgrades and process changes. The multiple injectors allow the sequential deposition of an SiO_2 diffusion barrier followed immediately by the SnO_2 coating. It has been observed that there is much

less debris incorporated into the films when both SiO_2 and SnO_2 are deposited in one pass, when compared to a multiple pass process.

Properties of the SiO_2 and SnO_2 films deposited in this system are shown in **Table 2.1.** The range of properties shown in this table cover the parameter space in which most of our work has been carried out; it is possible to achieve a wide range of properties by varying process conditions.

One area of the furnace that works particularly well is the dopant system. Sheet resistances as low as 6.6 ohm/square have been obtained from films that were only 540 nm thick. These data indicate that the resistivity of the tin oxide film is 3.6×10^{-4} ohm-cm, about half the resistivity obtained with our standard process. This capability allows us to explore lower sheet resistance films and thus will allow us to reduce resistive losses in our multi-junction modules.

PROPERTIES OF FILM DEPOSITED IN THE LARGE-AREA APCVD FURNACE		
FILM TYPE	**THICKNESS* (nm)**	**SHEET RESISTANCE* (ohm/square**
SiO_2	40 - 80	-
Specular SnO_2	200 - 400	10 -50
Textured SnO_2	500 - 1500	5 - 30
*Properties can be varied based on process conditions		

Table 2.1

2.3 Injector Design

A uniform injector is the heart of a reliable APCVD furnace. Considerable work has gone into the development of an injector design. At present, the results have been somewhat mixed for the two components that make up the injector, the injector head and vent assembly.

The injector head is the component that takes the reactant gases from a single point source (i.e., the inlet tube) and distributes it uniformly across the width of the substrate. This component is the most critical and is the area where we are having the most trouble.

During this phase we have built, tested and modified a prototype injector head several times and made significant improvements along the way. However, we still have excessive film thickness variation caused by a non-uniform distribution of reactive gases across the width of the substrate. We have identified several potential problems with our current design and have developed a fully documented design for a production unit that addresses each of our problems. It is expected that this new design will provide the uniformity we require.

The function of the vent assembly is to take the reacted gases from the injector head and exhaust them from the substrate to the exhaust system and ultimately to the gas scrubber. The vent assembly that was designed, fabricated and tested during this phase has worked well thus far. It does a good job of removing the reacted gases and has not contributed to debris in the tin oxide films.

A schematic drawing of the injector head with the vent assembly is shown in **Figure 2.1.**

2.4 Process Optimization

The focus of our process optimization work has been on improving the consistency of our film properties throughout a run, and maintaining uniform thickness across a 0.41 m (16 in) width on our large-area APCVD furnace.

Figure 2.2 shows the sheet resistance, percent haze and percent transmission (measured in air) of a typical run of tin oxide used for our multi-junction development work. The properties of the tin oxide do not drift significantly during a run. The system reaches steady state and generally does not drift as long as all process variables are in control.

As mentioned previously, the uniformity of the APCVD injector is critical to the success of an APCVD furnace. During this phase, both process and equipment changes were made to improve the uniformity of the thickness of our tin oxide.

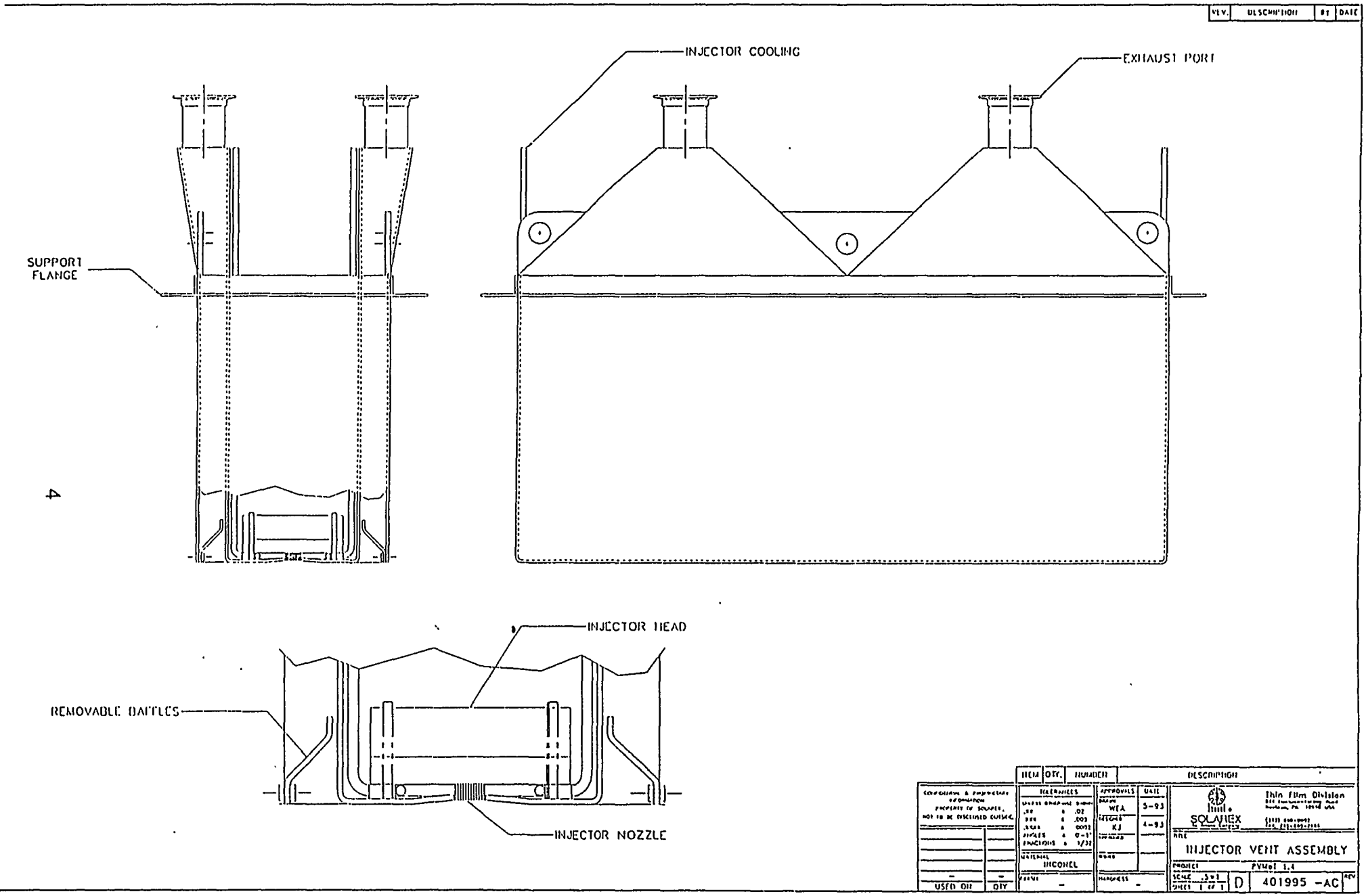

Figure 2.1. Schematic drawing of injector head with vent assembly.

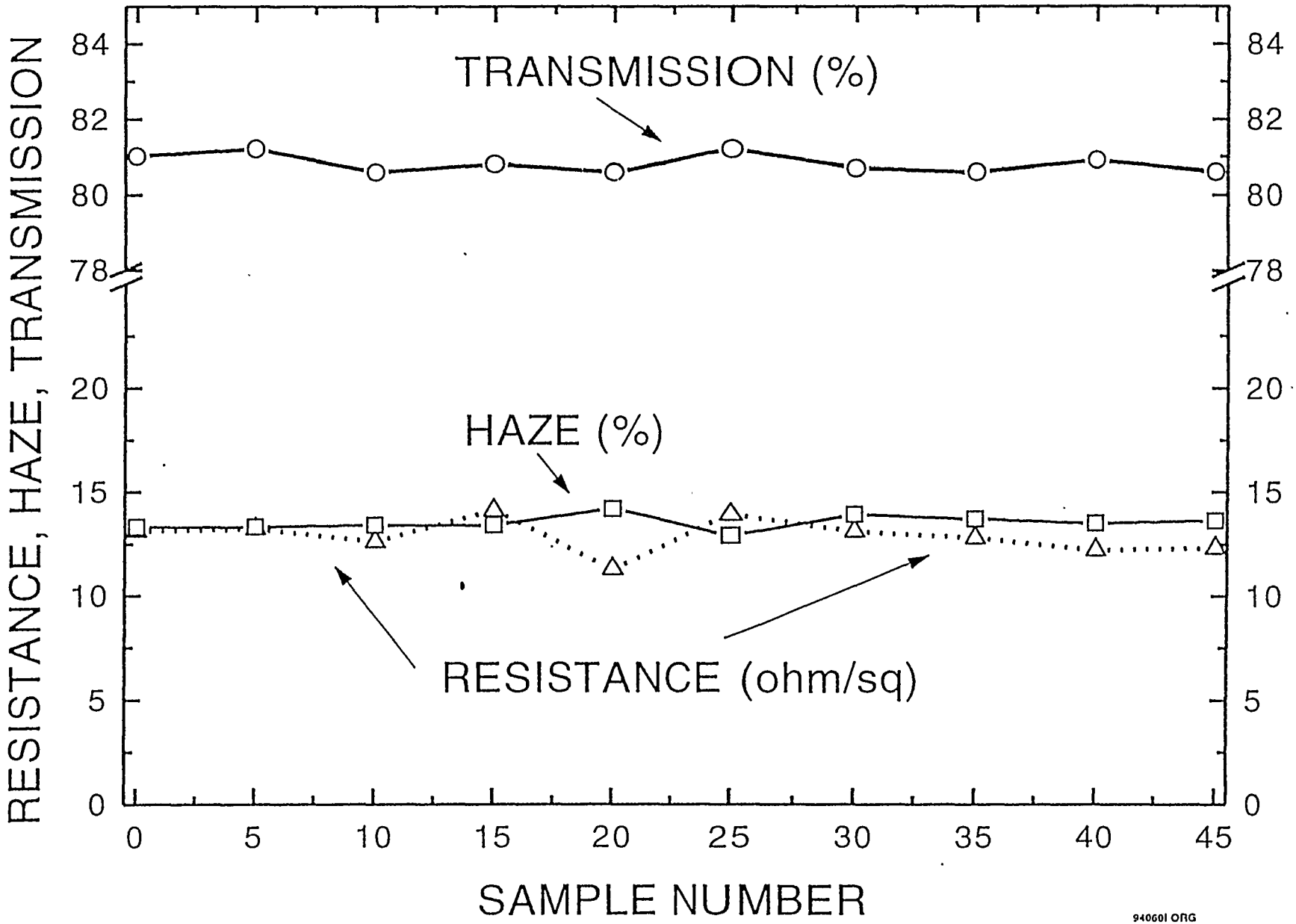

Figure 2.2. Properties of a typical run of tin oxide used for multi-junction development.

The process factors contributing to the film non-uniformity were identified by running several sets of designed screening experiments. By using this method, we reduced many variables that could potentially affect film uniformity to four significant factors (tin IV chloride flow, tin: methanol ratio, reactant gas temperature and feedstock gas flow uniformity at the injector nozzle). Because of these experiments, the film uniformity has been improved on 70% of the width of the substrate. (See **Figure 2.3**). The remaining film non-uniformity is due to equipment limitations in the injector head. New designs have been proposed to eliminate this remaining problem.

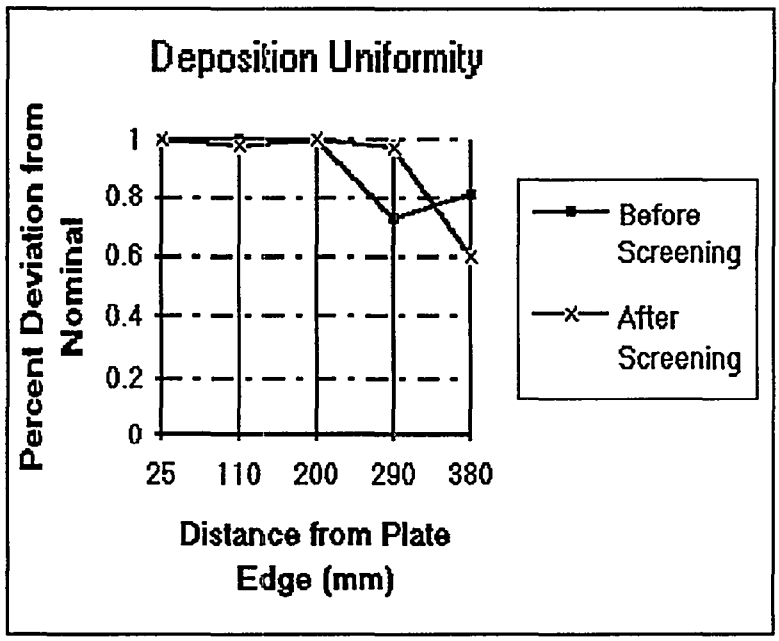

Figure 2.3. Improvement in deposition uniformity.

2.5 Alternate Materials

To improve module performance, increase manufacturing safety and reduce production costs, several alternate feedstock materials have been evaluated. Thus far, there have been encouraging results in alternate materials for the fluorine dopant, the tin feedstock, and in replacing tin oxide with zinc oxide.

2.5.1 Alternate Fluorine Dopant

The large-area APCVD furnace is equipped with a proprietary dopant system that allows us to achieve very good fluorine incorporation in our tin oxide without having to handle corrosive or toxic dopant gases. During this phase, we identified and tested a dopant gas that is safer than our previous dopant gas. It is also less expensive (cost is less than 1¢ per m^2 of tin oxide). This material has been adopted as our standard dopant and has shown itself to be reliable over long periods.

2.5.2 Alternate Tin Feedstock

Laboratory scale tests have been completed on a third party proprietary tin feedstock for making tin oxide. This material has been used successfully in the bottle coating industry, where a thin layer of tin oxide is used to improve lubricity and abrasion resistance for high speed bottle-filling operations. Working with the manufacturer, we have shown that this material can also be used to make conductive tin oxide films with properties required for thin film solar devices.

The films deposited during these tests have properties as follow:

R_{Sheet}	=	3.4-4.1 ohm/sq
Haze	=	18-25%
Thickness	=	1160 nm
Transmission (in air)	=	78-80%

The above properties, although not optimized for our multi-junction devices, are good considering that this material is still in the early stages of its development. The sheet resistance is very low while the haze and transmission values are in the correct range for solar grade tin oxide. Prospects for further optimization are good as it appears that there is much to be gained in transmission by sacrificing some of the low sheet resistance. This would be done by making the tin oxide thinner or adding less dopant. Either approach will push the transmission well above 80% and thus improve device efficiency.

An additional benefit of this feedstock is that it allows all of the reagents to be mixed before entering the injector head. This allows a much simpler injector head to be designed which lowers the capital cost of the equipment significantly and improves reliability, while reducing the risks involved in developing a complex injector head.

2.5.3 Zinc Oxide Alternative

Zinc oxide has been explored as an alternative to tin oxide as a means to improve the transmission of the front contact. Two approaches were explored for depositing zinc oxide. The first is the high deposition rate APCVD from diethylzinc (DEZ), similar to our tin oxide process. The second process is low pressure chemical vapor deposition (LPCVD) from DEZ.

The APCVD of zinc oxide using DEZ met with mixed results. Specular films doped with fluorine were fabricated with excellent conductivity and uniformity (7 ohm/square, 800 nm thick); the textured films resulted in powder formation and optical non-uniformities. Day to day variations were common which clearly indicated that there were some important variables that were not being controlled. The most repeatable results were obtained with process conditions that controlled the deposition rate limiting step, the diffusion of the gases to and from the substrate. The transmission of the best zinc oxide films offered significant improvements over tin oxide, as shown in **Table 2.2.** The gas diffusion could not be controlled well enough, so the films were never reliably uniform.

In an attempt to control the gas diffusion to the substrate, LPCVD was examined. The result was extremely uniform films over a 0.10 m^2 (1 ft^2) area (see **Table 2.2**). The films were tested by making electrical and optical measurements and making solar cells. It became apparent from these measurements that the zinc oxide was superior when evaluated apart from a solar cell, but when incorporated into a device, there were other problems that needed to be addressed (e.g., low V_{oc} and fill factor). Assuming these device issues can be addressed, we expect to see a 5-10% increase in performance due to higher currents, resulting from the improved transmission.

The process and equipment reliability of the LPCVD process are currently being evaluated using a 0.10 m^2 (1 ft^2) system. This information is being used to gather the information required to build a reliable large-area system suitable for use in a high production facility. Information is being collected on preventive maintenance schedules, process repeatability and equipment/design improvements. As these items are identified, they are being incorporated into the large-area designs.

The initial large-area zinc oxide system designs are complete; fabrication of the system has begun. The system has been designed to serve our zinc oxide needs for both front and rear contacts, and is currently scheduled for completion well before our original December 1994 target date.

COMPARISON OF APCVD TIN OXIDE TO APCVD AND LPCVD ZINC OXIDE			
PROPERTY	**APCVD TIN OXIDE**	**APCVD ZINC OXIDE**	**LPCVD ZINC OXIDE**
Sheet Resistance (ohm/square)	13	14	14.5
Haze*	24	15	19
Transmission*	79	83	83-85
Thickness (nm)	840	860	1,500
Uniformity	Good	Poor	Very Good
*Measured in air on Gardner XL-211 Hazegard system.			

Table 2.2

3.0 TASK 9: LASER SCRIBING PROCESS DEVELOPMENT

3.1 Introduction

During this period we have demonstrated laser scribe processes capable of throughput rates of 30 plates per hour with an area utilization of over 94%. Laser scribe rates of 0.3716 m^2 per minute (4 ft^2 per minute) have been demonstrated on 0.557 m^2 (6 ft^2) substrates for all four of the scribing processes: tin oxide scribe, amorphous silicon scribe, metal scribe and isolation scribe. Total scribe widths of less than 676 μm (0.0266 in) have been attained at this high throughput rate. Upgrades to the large-area laser scribe system made during this period were essential to attaining high throughput processes and a high area utilization.

3.2 Optimization of Laser Scribe Process

The purpose of laser scribe processes is to electrically isolate solar cell material into segments and selectively remove material so that subsequent processing results in an electrical series connection between adjacent segments. In addition, for monolithic substrates the laser isolation scribe serves to electrically isolate the segments of a module from the edges of the substrate. Laser scribing processes must meet several requirements to be effective. First, laser scribe processes must remove one layer of material without removing or damaging the other layers that make up the solar cell. Second, the width of the laser scribes should be as small as possible to maximize the area of photo-active material on the module substrate. Third, the positioning of the scribes must be precise to

maximize the photo-active area and to prevent crossing scribes. Finally, the speed of scribing should be as high as possible to maximize the throughput of the laser processes.

Laser scribe processes are based on transferring sufficient energy into the material so that the material is vaporized. The laser scribe process requirements mentioned above can be achieved in part by adjusting the process parameters to maximize this selective energy transfer. One approach to maximizing this energy transfer is to use a laser that emits light at a wavelength where the material to be scribed is highly absorbing. Since different layers of the solar cell structure are highly absorbing in different regions of the electromagnetic spectrum, matching the laser wavelength to the material to be scribed should aid in obtaining selective and efficient energy transfer to the material. In addition, higher energy transfer rates imply faster scribe speeds.

A major focus of this task in this period has been to optimize the laser scribe processes by establishing the effect of laser wavelength on the quality, speed and width of the resulting laser scribes. Laser wavelengths in the ultra-violet (UV), visible (VIS) and infrared (IR) regions of the spectrum were used to perform each of the laser scribe processes. All of the scribe types (tin oxide, amorphous silicon, metal and isolation) were investigated. As a first step, the laser scribing parameters were varied to obtain a good quality scribe at each combination of scribe type and laser wavelength. Once the viability of the scribe had been established, the laser scribe parameters were varied systematically to determine the settings that would result in the highest speed and the smallest scribe width possible while maintaining scribe quality.

Examples of the range in scribe widths achieved are shown in **Figure 3.1** and in **Figure 3.2.** These figures are photographs of tin oxide scribes made using two different wavelengths of laser light. **Figure 3.1** is a tin oxide scribe of width 18 μm (7×10^{-4} in) produced using laser light in the ultraviolet region of the spectrum. **Figure 3.2** is a tin oxide scribe of width 3.8 μm (1.5×10^{-3} in) produced using laser light in the visible region of the spectrum. **Figures 3.1 and 3.2** illustrate the range of scribe widths that can be achieved by changing the laser wavelength. For a laser operating at a fixed wavelength, it is possible to change the width of a laser scribe and the speed at which the scribe is done by changing various scribe parameters. However, we have found that by using lasers of different wavelengths, it is possible to significantly increase the range over which the width of a scribe can be adjusted, and increase the range of scribe speed.

This work, together with several laser system upgrades, have resulted in laser scribe processing speeds of 30 plates per hour and an active area utilization of 94% on 0.372 m^2 modules. **Figures 3.3 - 3.5** are photographs of a tin oxide scribe, a metal scribe, and an isolation scribe done on 0.406 x 0.9137 m (16 x 36 in) substrates. Each of these scribes was done at a processing speed of 4 ft^2 per minute. **Figure 3.6** is a photograph of a tin oxide scribe, an amorphous silicon scribe and a metal scribe on a 0.406 x 0.9137 m (16 x 36 in) substrate. The total scribe spacing on this module is about 674 μm (0.0266 in) resulting in an area utilization of over 94% on this module. Further optimization of laser scribe parameters including laser wavelength is planned.

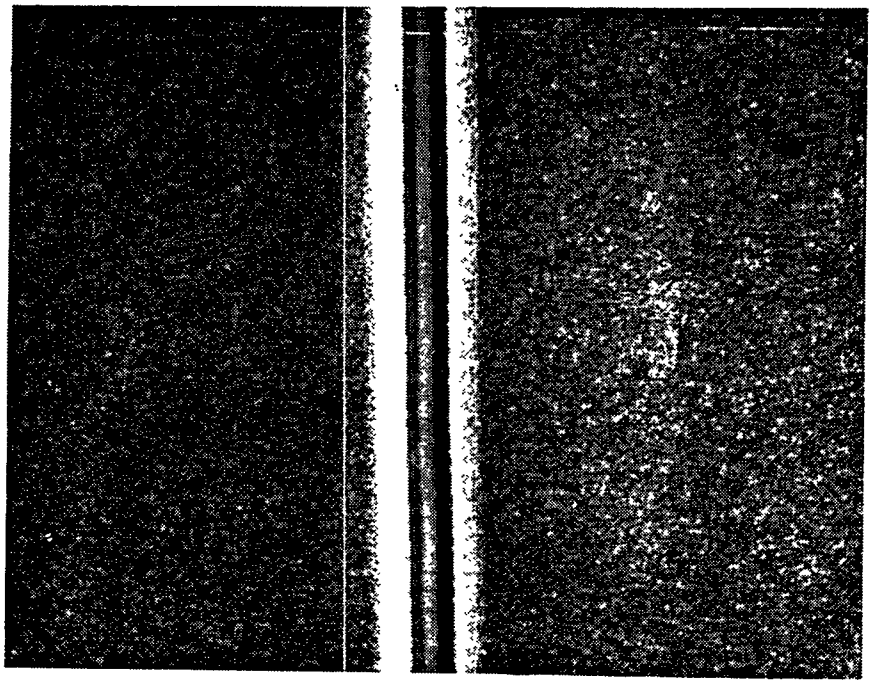

Figure 3.1. Photograph of a 1.78 x 10^{-3} cm (7 x 10^{-4} in) wide tin oxide scribe

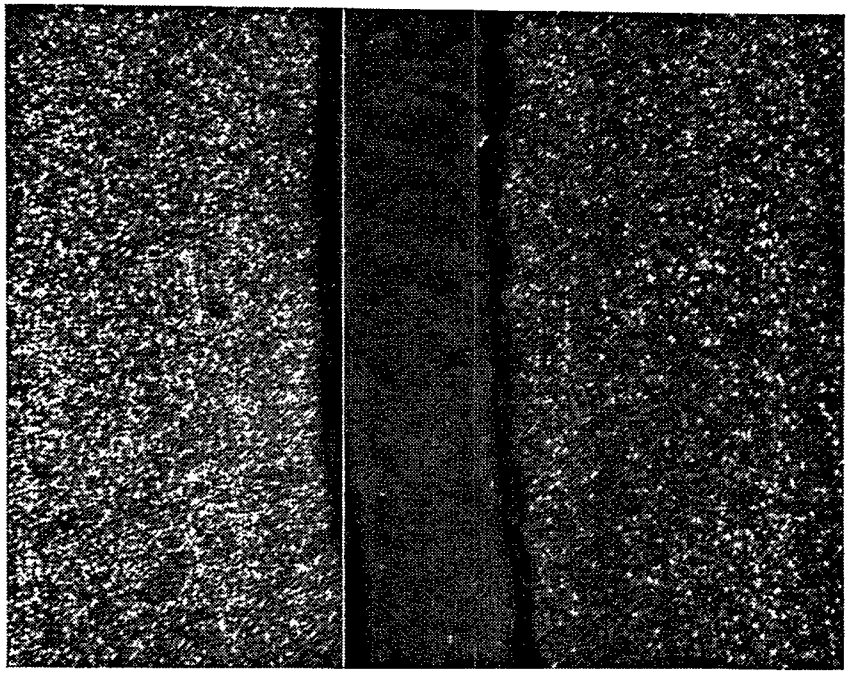

Figure 3.2. Photograph of a 3.3 x 10^{-3} cm (1.3 x 10^{-3} in) wide tin oxide scribe

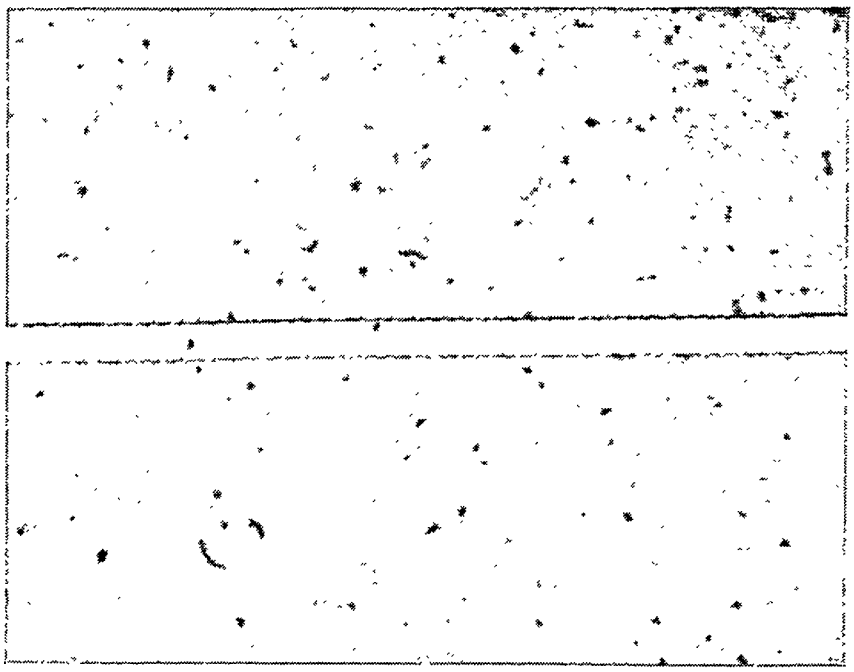

Figure 3.3. Photograph of a tin oxide scribe done on 0.406 x 0.913 m plate at a rate of 4 ft^2 per minute

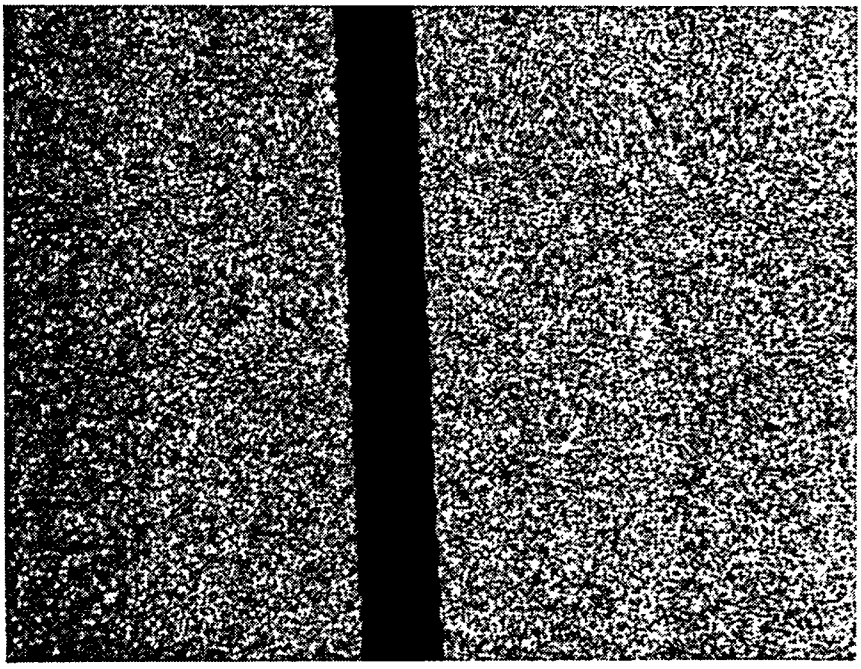

Figure 3.4. Photograph of a metal scribe done on 0.406 x 0.913 m plate at a rate of 4 ft^2 per minute

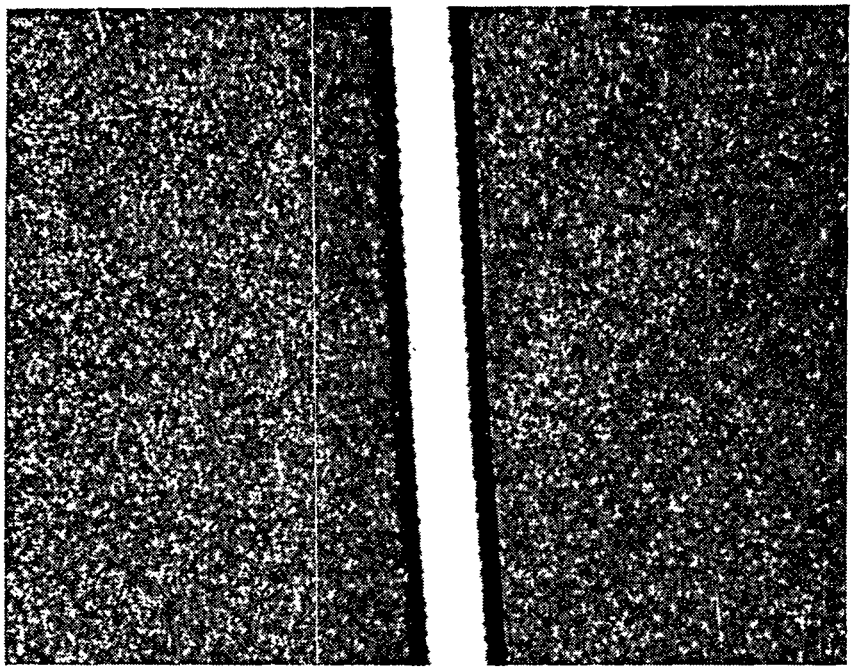

Figure 3.5. Photograph of an isolation scribe done on 0.406 x 0.913 m plate at a rate of 4 ft^2 per minute

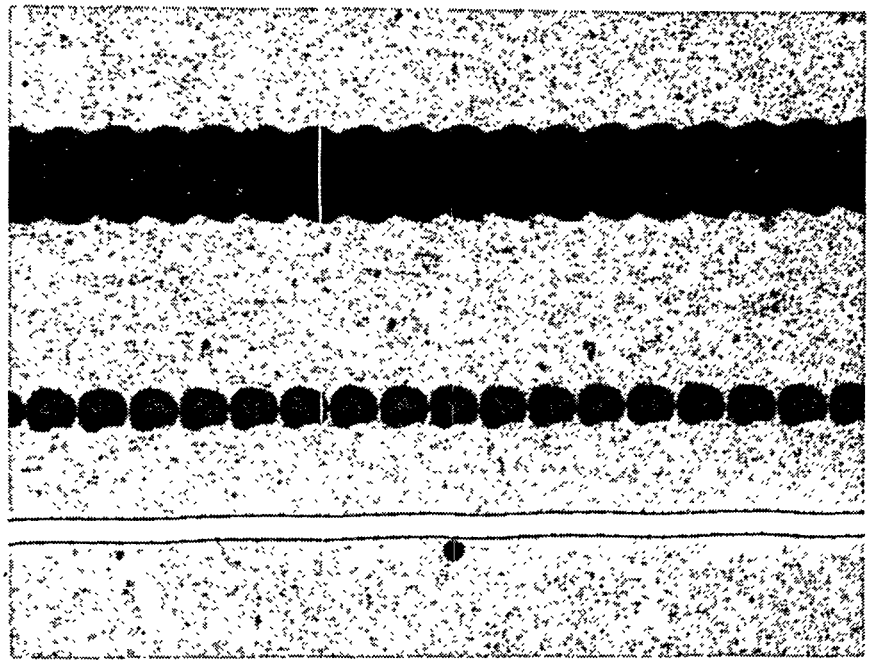

Figure 3.6. Photograph of tin oxide, silicon and metal scribes on a 0.406 x 1.913 m size module. The total width of the scribe is 0.533 mm (2.1×10^{-2} in)

3.3 Laser System Improvements

The results presented in **Figures 3.3 - 3.6** were obtained on a large-area laser scribe system capable of scribing 0.5574 m^2 (6 ft^2) plates. In this period, several modifications were made to this system. These modifications were essential to attaining the results presented in the figures. Linear motion components were upgraded to reduce the laser beam drift per linear inch of travel and to increase the precision of beam positioning on the plate. These modifications led to an increase in the active area utilization on a module. In addition, this system was converted to a dual-beam laser system, effectively cutting the scribe time per plate by a factor of two.

4.0 TASK 10: AMORPHOUS SILICON BASED SEMICONDUCTOR DEPOSITION

4.1 Introduction

During this period, Task 10 efforts were concentrated in two major areas. In the area of equipment development, we completed the design and construction of a large-area amorphous silicon deposition system, capable of handling substrates up to 0.74 m^2 (8 ft^2) in area. This large-area deposition system was used to evaluate several reactor design concepts directed at obtaining uniform film deposition over large areas. After several modifications, we have deposited amorphous silicon films with a thickness uniformity of ± 3.1% over 0.74 m^2 (8 ft^2) substrates.

Besides our equipment development efforts, we have continued our triple-junction process development. Triple-junction module recipes have been transferred from research equipment to deposition equipment capable of handling substrate sizes up to 0.37 m^2 (4 ft_2). Our process development efforts have resulted in a triple-junction module with an initial conversion efficiency of 10.3% on an area of 0.1 m^2 (1.08 ft^2) and a triple-junction module with an initial conversion efficiency of 8.12% on an area of 0.37 m^2 (4 ft^2).

4.2 Large-Area Equipment Development

4.2.1 Equipment Considerations for Large-Area Deposition

A major equipment development challenge is to design and build chambers such that the deposition of the amorphous silicon films is extremely uniform over large areas. This is particularly important with multi-junction device structures where the tunnel junction layers are both critical to the device performance and are also very thin. As the size of the chambers is increased, several related factors must be considered to obtain uniform film deposition. The distribution of the reactant gases inside the reactor will significantly influence the uniformity of deposition. At process pressures, large-area reactors have overall

dimensions that are several times the mean free path of the gas molecules. Consequently, it is possible to create localized non-uniformity in the process gas mixtures as well as in total gas pressure. The degree to which these non-uniformities exist will depend upon how these gases are fed into and pumped from the reactor. In addition to non-uniform gas distribution, non-uniform substrate temperature can also cause variations in film properties. To obtain the highest processing throughput the substrate heaters must be designed to bring the temperature of the substrate to the desired value as quickly and as uniformly as possible. A third design consideration is uniform spacing between the substrate and the plasma-exciting electrodes. As the reactor size is increased, these spacing requirements become increasingly tight. In addition, this uniform geometric spacing must be maintained as the reactor parts and the substrate are heated and cooled. One additional concern in scale up of the amorphous silicon reactor is to minimize the residence time of gas throughout the reactor. As chambers become larger, the time required to purge the chamber of dopant gases may increase, thus requiring longer flush times between doped and intrinsic layers.

4.2.2 Equipment Development

In a previous period, we reported on a five-chamber, large-area deposition system design. This system design incorporated several features aimed at addressing some of the challenges associated with scale-up of amorphous silicon deposition to large areas. Our overall equipment development approach was to install all of the deposition equipment subsystems on the large-area machine and use a single deposition chamber to evaluate our proposed design features. Once the design of the deposition chamber was finalized, the other deposition chambers would be modified accordingly. The advantage of this approach is that evaluation of the deposition chamber design could begin prior to completing the overall system.

All of the major subsystems have been installed on the large-area system. The chambers were integrated, the vacuum subsystems have been completed, the gauges have been installed, and the transport for the complete system is operational. The exhaust systems and gas manifolds have been installed, and all of the major subsystems have been debugged.

Our deposition chamber scale-up evaluation began with the design and fabrication of prototype cathodes, showerheads and substrate holders. A major departure from previous systems was the choice of material used to fabricate these components. In previous systems, molybdenum was used exclusively to fabricate these parts. The primary advantages of molybdenum are its strength, thermal stability and the match in thermal coefficient of expansion between molybdenum and the glass substrate. There are, however, several

disadvantages of molybdenum, particularly for scale-up to large areas. For example, raw molybdenum stock is typically not available in large sheets. Consequently, to build up sizable components, it is necessary to machine smaller pieces and assembly them into the complete component. Secondly, molybdenum is an expensive material and adds significant expense to the cost of building systems. In addition, since molybdenum is a porous material, it is difficult to clean properly. To overcome these difficulties, we have used titanium to fabricate our cathodes, showerheads and substrate holders for the large-area system.

We have found that titanium offers several advantages over molybdenum when used to fabricate deposition components for large-area machines. First, the cost of fabricating parts of titanium is approximately one-half of the cost of fabricating the same parts from molybdenum. Not only is the titanium raw material less expensive, but also the cost of machining titanium is lower. In addition, since titanium is available in larger sizes, one-piece components can be fabricated. This is a distinct advantage in maintaining the precise spacing between deposition chamber components required for uniform deposition.

A second unique feature of the large-area deposition system, is a six-zone substrate heater assembly on the lid of the deposition chamber. Prior heater assemblies utilized one to three zones, depending upon the system. These heater assemblies are sufficient for heating smaller size substrates, however, as the substrate size is increased, they become less efficient at obtaining a uniform temperature in a given time. We find that adding heat zones around the periphery of the substrate, results in increased flexibility and improved substrate temperature uniformity.

As part of our initial qualification of the large-area deposition chamber, we deposited single-junction device structures on 0.74 m^2 (8 ft^2) substrates. These films were characterized by measuring the thickness of the films at various points over the substrate and by metalizing samples of material taken from the substrate. Two problems were identified in these studies. First, the uniformity of deposition over the 0.74 m^2 (8 ft^2) area of the substrate was significantly worse than our target uniformity of ± 5%. Second, our device characterization indicated that due to a long gas residence time, the intrinsic layer had been contaminated with dopant material. Based on these studies, several modifications were made to this system. First, the gas manifolds were redesigned and rebuilt to separate the dopant materials from the intrinsic materials. Second, potential pockets of trapped gas in the manifold and the deposition chamber were identified and eliminated. Third, our multi-port gas distribution and gas pumping systems on the deposition chamber were augmented.

Multi-port gas distribution and pumping was originally designed into the large-area deposition system to obtain uniform gas distribution throughout the deposition chamber. A detailed study of the films thickness profile over the 0.74 m^2 (8 ft^2) substrate area suggested that this multi-port design was effective, but additional ports were required. The effect of these modifications are summarized in **Figure 4.1.** This figure shows the film thicknesses measured over the 0.406 m x 1.83 m substrate area. The average film thickness over this 0.74 m^2 area was 507.6 nm. The range in the thickness measurements was (523 - 491) or 32 nm. The thickness uniformity over this area is 507.6 ± 16 nm or 507.6 ± 3.1%. This result compares favorably to the ± 5% uniformity targeted for this system.

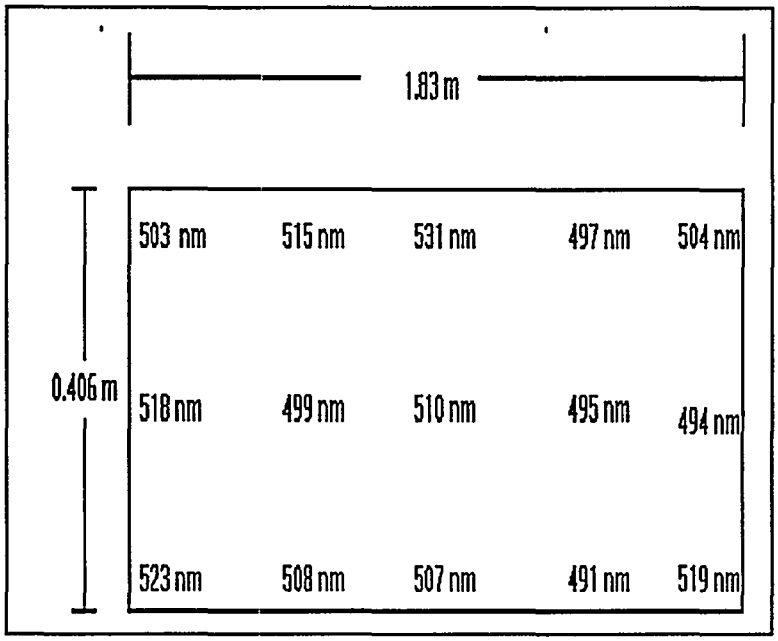

Figure 4.1. Film thickness profile of a film deposited in the large-area deposition system on a 0.74 m^2 (8 ft^2) substrate.

4.2.3 Module Development

In parallel with our equipment development efforts, we have continued our high performance triple-junction module development work. In the last period we reported that triple-junction module recipes were transferred from research machines to a machine capable of processing substrates with areas up to 0.37 m^2 (4 ft^2). During this period, we continued our high performance module development work in this machine. This machine was outfitted to hold three each 0.1 m^2 (1.08 ft^2) modules or one each 0.37 m^2 (4 ft^2) module in a single deposition run.

The basic solar cell structure of our high performance triple-junction modules is shown in **Figure 4.2.** The device structure is glass/textured tin oxide/a-Si:H/a-Si:H/a-SiGe:H/ZnO/Ag. A highly reflecting zinc oxide/silver rear contact is used to reduce the parasitic optical losses at the rear of the solar cell.

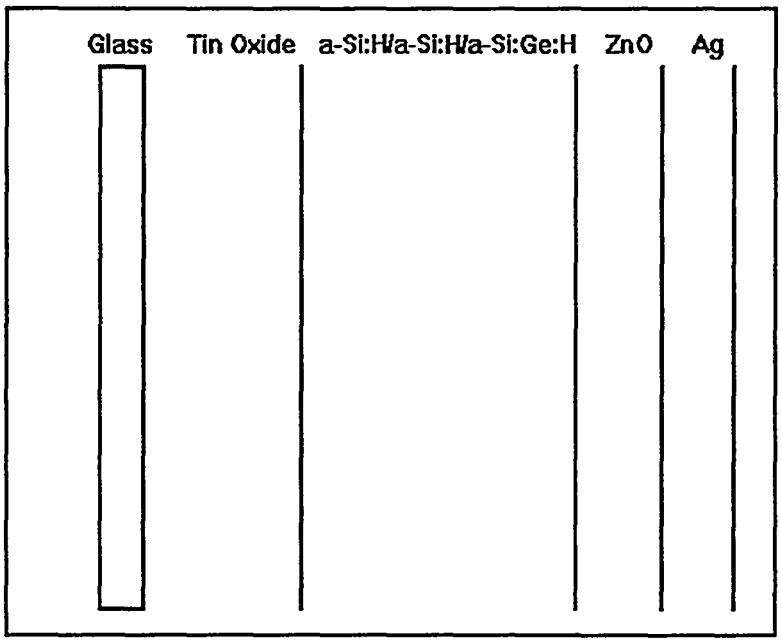

Figure 4.2. Basic structure of high performance triple-junction solar cell.

Our approach to large-area triple-junction module development was to use 0.1 m^2 modules as a diagnostic tool to improve the silicon layers and the basic module fabrication processes. After improvements were established on the 0.1 m^2 modules, these improvements were incorporated into the larger 0.37 m^2 (4 ft^2) modules.

Our progress is summarized in **Figure 4.3** and **Figure 4.4.** Figure 4.3 is an I-V curve of the best 0.1 m^2 (1.08 ft^2) module fabricated to date in our large-area development machine. This module has an initial aperture area conversion efficiency of 10.32% with the following photovoltaic parameters: V_{oc} = 62.98 volts, Isc = 218.5 mA and fill factor = 0.675. This module was made on low iron glass coated with our highly textured tin oxide. **Figure 4.4** is an I-V curve of a 0.37 m^2 (4 ft^2) fabricated in this same deposition system. This module has an initial aperture area conversion efficiency of 8.12% with the following photovoltaic parameters: V_{oc} = 84.64 volts, Isc = 564.9 mA and fill factor = 0.631. This 0.37 m^2 module was made on commercially available 3 mm thick tin oxide coated soda-lime glass. There are several reasons for the discrepancy between the performance of the 0.1 m^2 module and the 0.37 m^2 module. First, roughly 70% of the discrepancy

between the two modules can be attributed to optical losses at the front contact of the large-area substrate. Most of this optical loss is due to higher optical absorption in the soda-lime glass and the tin oxide. We expect that this loss will be eliminated once we have completed our large-area tin oxide development work. The second reason for the discrepancy between the two modules is the lower fill factor of the 0.37 m^2 module. Possible reasons for the loss in fill factor include higher contact resistance at the tin oxide/p-layer interface or at the n-layer/zinc oxide interface. In addition, there is some evidence to suggest that the tunnel junctions need to be re-optimized for the larger-area substrates.

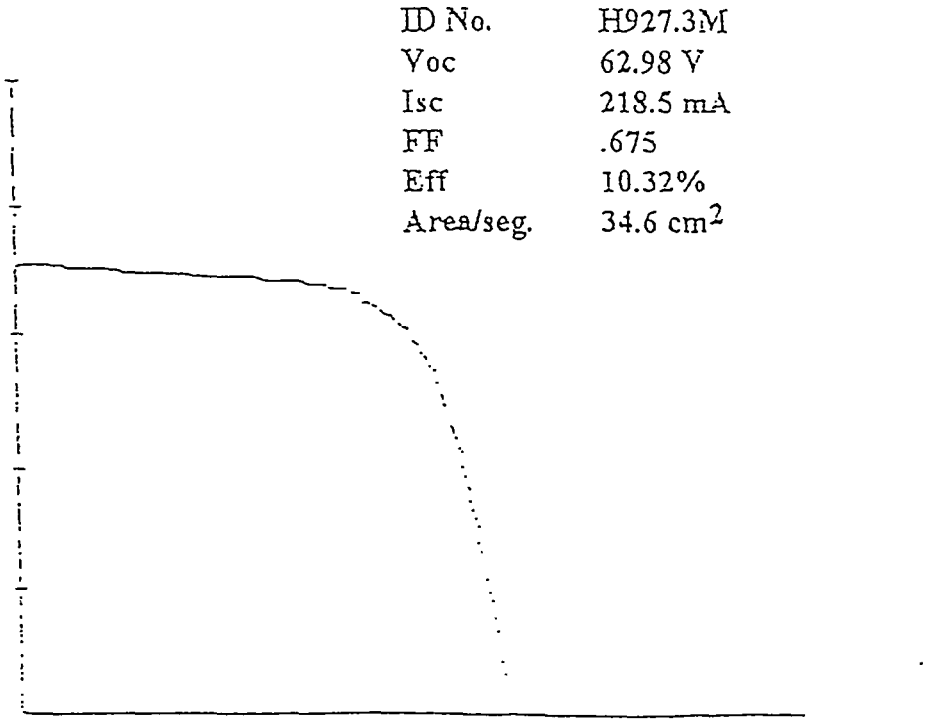

Figure 4.3. Initial I-V curve of a 0.1 m^2 (1.08 ft^2) triple-junction module.

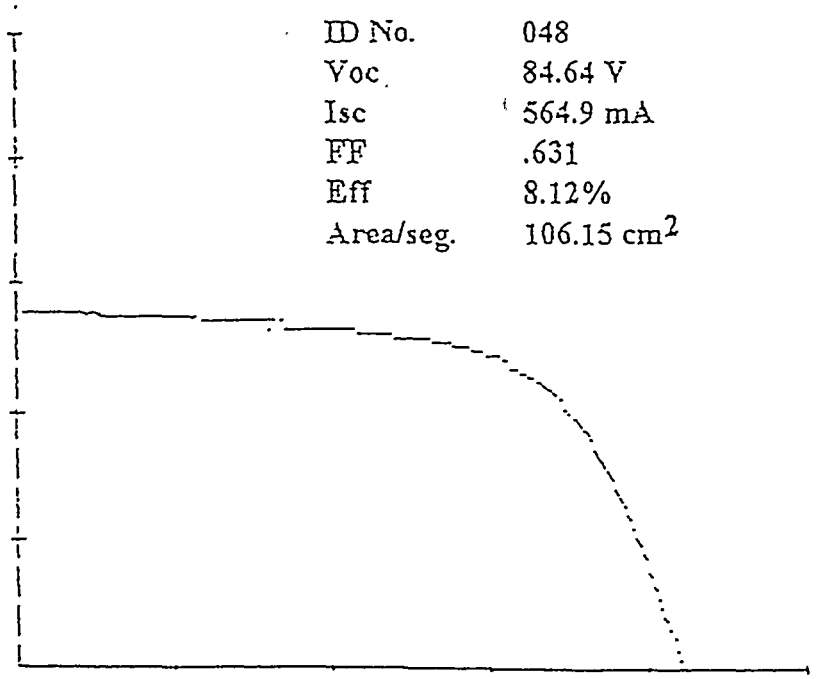

Figure 4.4. Initial I-V curve of a 0.37 m^2 (4 ft^2) triple-junction module.

5.0 TASK 11: REAR CONTACT DEPOSITION PROCESS

5.1 Introduction

During this period, two distinct zinc oxide deposition processes have been studied in the large-area metalization system. The first process that was investigated utilized a zinc oxide/aluminum oxide target as the source material. This process was done in the radio frequency (RF) magnetron sputtering mode with argon as the single sputtering gas. The second process utilized a zinc/aluminum alloy target as the source material. This second process was done in the direct current (DC) magnetron sputtering mode with a mixture of argon and oxygen as the sputtering gas. To help stabilize the discharge in this reactive process, a low frequency (400 kilohertz) RF voltage was impressed on the target.

Both processes have yielded highly transparent zinc oxide films suitable for use as a rear contact material. Uniform deposition of zinc oxide films on 16 in x 36 in substrates is possible with either deposition method. Quantum efficiency measurements done on single-junction devices have confirmed increased optical enhancement of zinc oxide/metal reflectors. We found that the deposition rate of the reactive process was approximately four times higher than that obtained by sputtering from an oxide target.

5.2 Zinc Oxide Deposition Processes

Each of the sputter deposition methods, from an oxide target and from a metal alloy target, has advantages and disadvantages. Sputter deposition from a low bulk conductivity target material such as zinc oxide is typically done using an RF generator operating at 13.56 megahertz (MHz) to maintain the discharge. Operating at such high frequencies however requires an impedance matching network to match the impedance of the sputtering discharge to the output impedance of the RF generator. Further, as the characteristics of the discharge change, the matching network must be retuned. Despite these complications, sputter deposition of zinc oxide from an oxide target has several advantages. Since the target material is oxidized, deposition of zinc oxide is solely a physical process, that is, the desired stoichiometry of the zinc oxide film is the same as that of the target. In addition, when sputtering from an oxide target, there are fewer process parameters to control. The process has been found generally stable over time.

In contrast to sputtering from an oxide target, sputtering from a metal target can be done using a direct current (DC) power supply. Since the target material is a metal, oxygen must be added to the discharge gas to form zinc oxide. This complicates the deposition process in at least two ways. First, there are additional process parameters to control, such as oxygen partial pressure and oxygen flow. Second, forming zinc oxide on the target surface causes variations in the discharge characteristics, in the stoichiometry of the target, and in the growing film. We have used an RF/DC combiner power supply to help stabilize the discharge characteristics and minimize these variations.

5.3 Zinc Oxide Deposition from an Oxide Target

Initial efforts to deposit zinc oxide films over large areas concentrated on sputter deposition from a zinc oxide/aluminum oxide target. Our large-area metalization system is a multi-chamber system with two deposition chambers separated by buffer chambers. The system has load and unload buffer chambers to minimize atmospheric contamination of the deposition chambers. Zinc oxide is deposited in the first deposition chamber and metals are deposited in the second deposition chamber. **Figure 5.1** is a schematic diagram of the zinc oxide deposition chamber. As indicated in this figure, the zinc oxide target is oriented in a sputter-up configuration. A 500 watt RF generator is connected to the target through an impedance matching network. The gas entry port is at the rear of the machine and off center. Substrates enter the deposition chamber through a slit valve at the left and are continuously transported left - to - right through the machine.

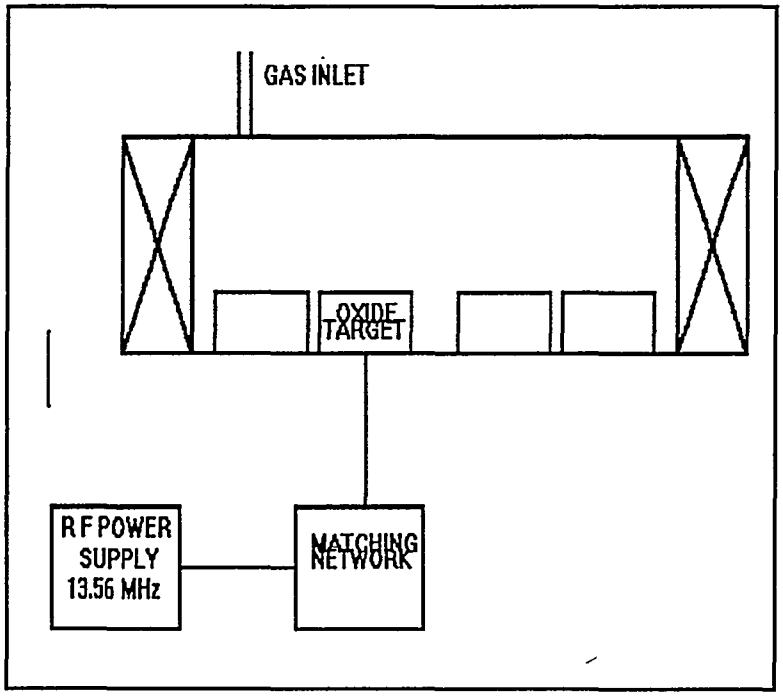

Figure 5.1. Schematic diagram of large-area metalization zinc oxide deposition chamber.

Prior to initiating process development work, the large-area system was qualified by using it to deposit aluminum rear contacts on single-junction solar cells. After qualification and some preliminary trials, the zinc oxide deposition parameters were varied systematically to determine the effect of these parameters on the zinc oxide film. Zinc oxide films were deposited on 16 in x 36 in glass substrates to determine the uniformity of deposition. The optical transmission of the films was determined by cutting a 2-inch square sample from the larger substrate. Transparent films with a nominal thickness of 35 nm are obtained at the following process settings: argon pressure - 3.5 millitorr, RF power - 500 watts, substrate temperature - 120 °C and transport speed of 8 linear inches per minute.

Figure 5.2 is the reflection spectrum of a zinc oxide/silver reflector deposited on glass. The zinc oxide was deposited as described above. The thickness of the silver film is 200 nm. This sample was cut from a 16 in x 36 in substrate and represents the reflection measured at various locations over the substrate. The reflection was measured in air with the light incident on the glass. Although a particular value of reflectance at any wavelength is due in part to optical interference phenomena, the generally high level of reflectance suggests the optical absorption of the zinc oxide film is low.

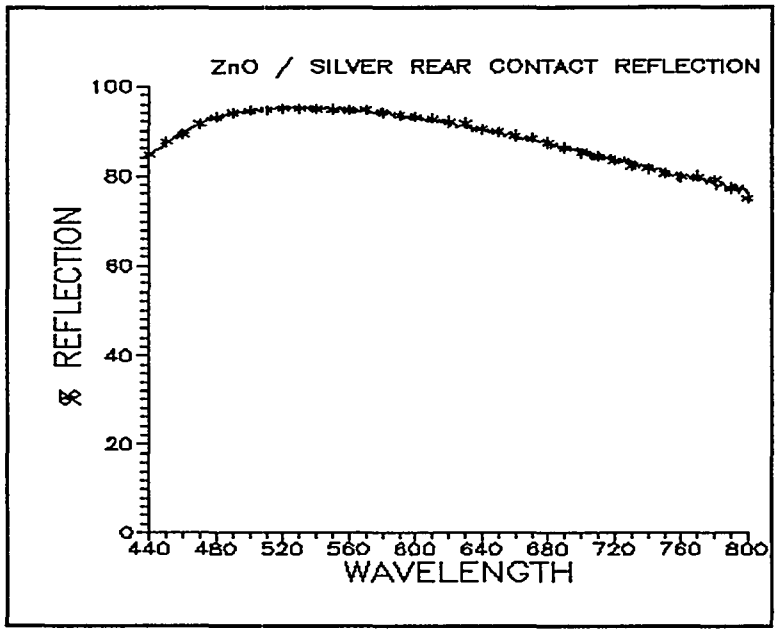

Figure 5.2. Reflection of a zinc oxide/silver reflector sample taken from a 16 in x 36 in substrate. The zinc oxide was deposited by RF magnetron sputtering from a zinc oxide target. The measurements were taken with the light incident on the glass surface.

To evaluate this zinc oxide/silver reflector, a comparison of single-junction solar cells metalized in the large-area system with equivalent solar cells metalized in one of our research systems was made. A summary of the resulting photovoltaic parameters measured on these solar cells is given in **Table 5.1.** A comparison of the quantum efficiency measurements made on these devices is given in **Figure 5.3.**

Inspection of **Table 5.1** and **Figure 5.3** suggest that there is no detectable difference in the long wavelength response of the devices. The average fill factor of the devices metalized in the large-area machine, however, tended to be slightly lower than the average fill factor of the devices metalized in the research system. Subsequent comparisons confirmed this result. This result led to further optimization of the substrate temperature in the large-area machine. After optimizing the substrate temperature, similar paired comparisons using additional samples of a-Si:H substrates were made. One such comparison study is summarized in **Table 5.2.**

SYSTEM	AVG. V_{oc} (Volts)	AVG. J_{sc} (ma/cm$^{2)}$	AVG. FILL FACTOR
Large-Area System	0.867 ± 0.010	13.77 ± 0.02	0.611 ± 0.027
Research System	0.874 ± 0.005	13.79 ± 0.06	0.650 ± 0.029

Table 5.1. Comparison of photovoltaic parameters for single-junction solar cells metalized in a research system and in the large-area metalization system. The rear reflector for all solar cells is zinc oxide/silver. The short circuit current densities were determined from quantum efficiency measurements. The errors are the standard deviations in the measurements.

SYSTEM	AVG. Voc (Volts)	AVG. Jsc (ma/cm^2)	AVG. FILL FACTOR
Large-Area System	0.889 ± 0.003	12.45 ± 0.05	0.621 ± 0.006
Research System	0.886 ± 0.003	12.34 ± 0.05	0.627 ± 0.020

Table 5.2. Comparison of photovoltaic parameters of single-junction solar cells metalized in the large-area metalization system to those metalized in a research system. The short circuit current densities were determined from quantum efficiency measurements.

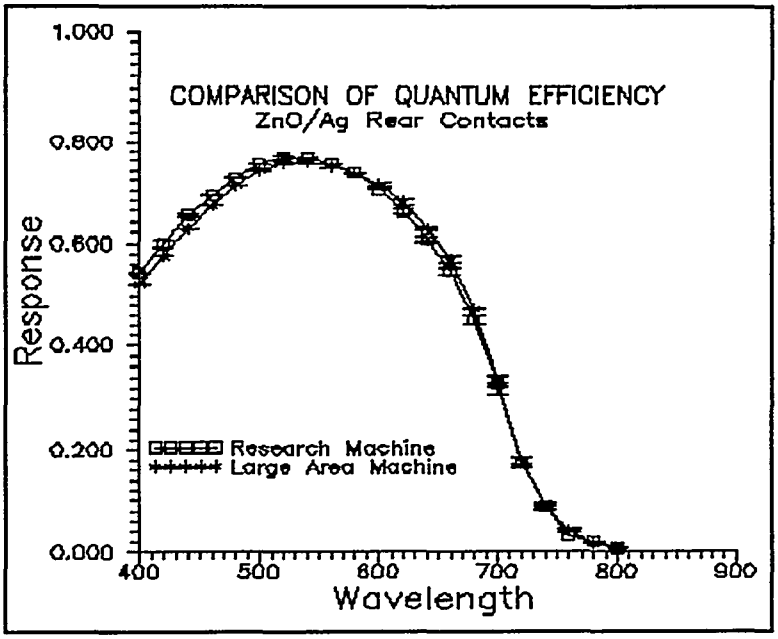

Figure 5.3. Comparison of quantum efficiency measurements of single-junction solar cells metalized in a research system.

5.4 Reactive Sputtering of Zinc Oxide

Reactive sputtering of zinc oxide from a metal alloy target has several advantages over sputtering from an oxide target. For the same size target, fabricating a metal target is not as complex as fabricating an oxide target. Consequently, metal targets are less expensive than oxide targets. In addition, the deposition rate from DC magnetron sputtering is usually significantly higher than is obtained using RF magnetron sputtering.

The advantages of a reactive sputtering process are partially offset by the increased complexity of reactive sputtering. If a reactive gas is introduced into a sputtering discharge, the characteristics of the discharge may vary significantly due to the chemical reactions that occur at the target surface. The variations in discharge parameters and variations in the target surface may be evidenced in poor process repeatability and in variation of the film properties.

We have successfully employed a combined AC/DC discharge and a zinc/aluminum metal alloy target to deposit zinc oxide films over large areas. The combination of alternating current and direct current voltage impressed on the target, has helped to maintain the stability of the discharge and has led to higher deposition rates than are obtained in RF sputtering. The configuration of the deposition chamber used to reactively sputter zinc oxide films is diagramed in **Figure 5.4.**

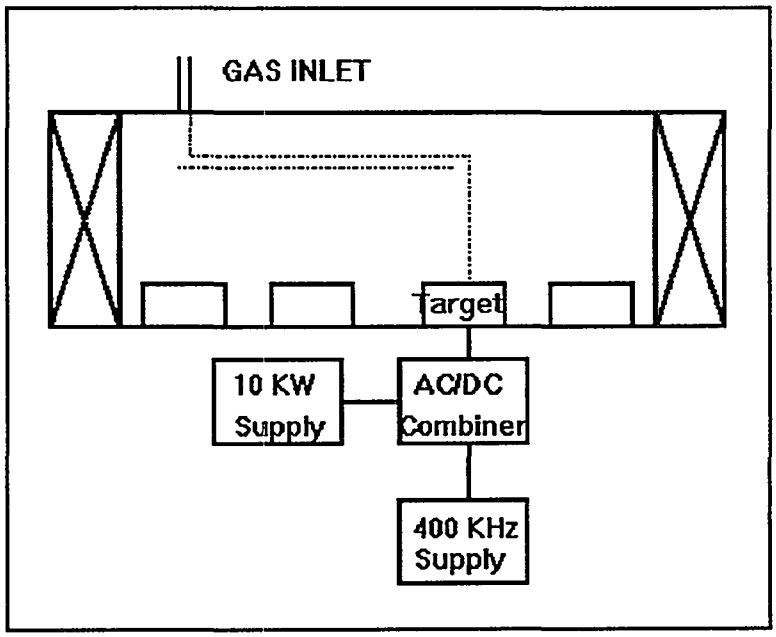

Figure 5.4. Configuration of the deposition chamber for reactive sputtering of zinc oxide films.

The AC/DC combiner adds the output of a 10 kW DC power supply to the output of a 2.5 kW RF supply. The RF supply operates at a frequency of 400 kHz which is a significantly lower frequency than 13.56 MHz. At this frequency no additional tuning is required after an initial tuning setup. The combiner permits a wide range of voltages to be impressed on the target including only RF or only DC voltages. In addition, the relative ON TIME and OFF TIME of the RF output can be adjusted.

After initial trials, the process parameters were varied systematically to determine the effect of these parameters on the zinc oxide film properties. **Figure 5.5** summarizes the results of one study. For each combination of input parameters, the optical transmission of the film was characterized as CLEAR, YELLOW or DARK OXIDE. Over the range of values tested, the RF power to the target was the most significant input parameter. As shown in **Figure 5.5**, the optical transmission of reactively sputtered zinc oxide exhibited a sharp decline at an RF input power of approximately 1 kW. The effect of RF power on the sheet resistance of the zinc oxide films is shown in **Figure 5.6**. Based on the results shown in **Figure 5.5** and **Figure 5.6**, the RF power to the target was reduced below 500 watts in subsequent investigations.

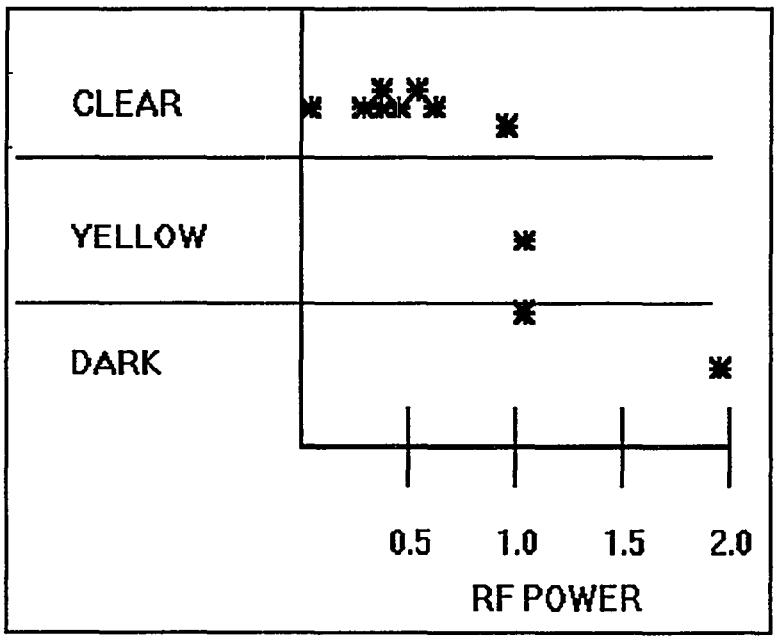

Figure 5.5. Effect of RF power on the optical transmission of reactively sputtered zinc oxide films.

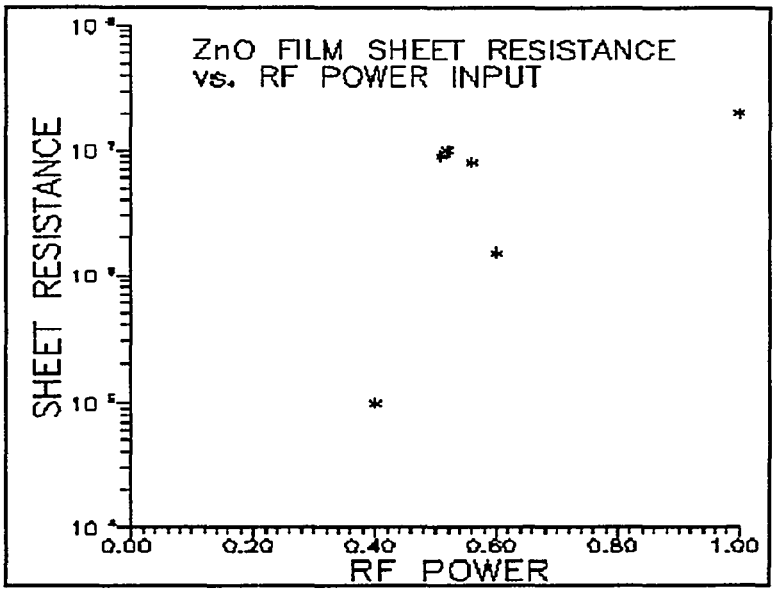

Figure 5.6. Effect of RF power on sheet resistance of reactively sputtered zinc oxide films.

Reactively sputtered zinc oxide deposited on 16 in x 36 in substrates exhibited a darker band of material extending along the length of the substrate. Two modifications were made to the deposition system to eliminate this darker region. Longer substrate heaters were

installed and the gas delivery manifold was extended to the target shroud. After re-optimizing the process to compensate for these two changes, uniform, conducting films with high transmission were obtained. Representative transmission and reflection measurements of reactively sputtered zinc oxide films, are given in **Figure 5.7.**

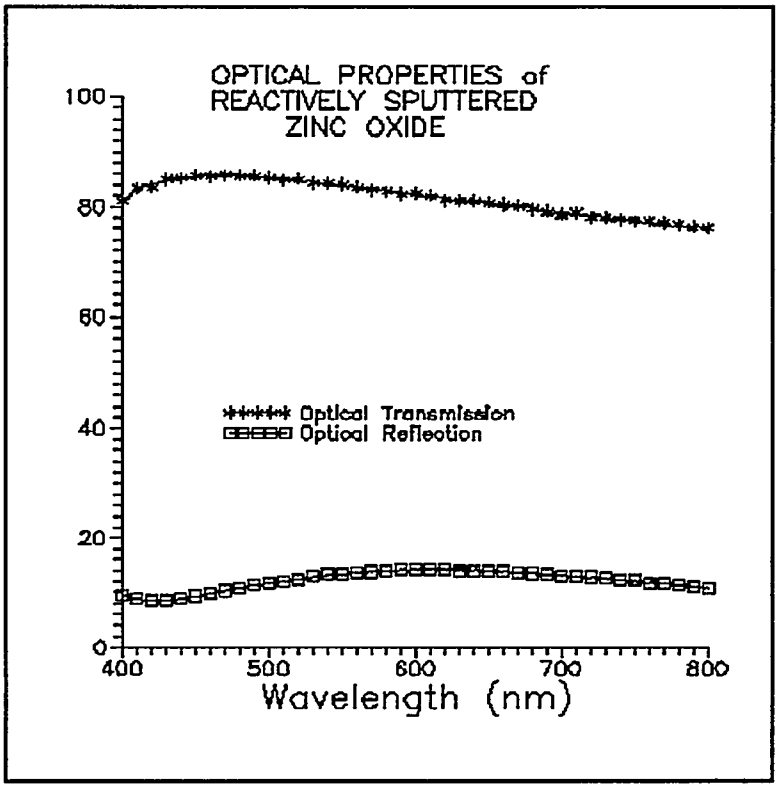

Figure 5.7. Optical transmission of reactively sputtered zinc oxide film.

These measurements shown in **Figure 5.7** were done on a sample cut from a 16 in x 36 in glass substrate. If the optical transmission measurement is corrected for the air/film, film/glass and glass/air interfaces, the corrected transmission shown in **Figure 5.8** is obtained. The peak optical transmission of the reactively sputtered zinc oxide film is well over 90%. The thickness of this film is approximately 100 nm. This film has a sheet resistance of 70 ohms per square.

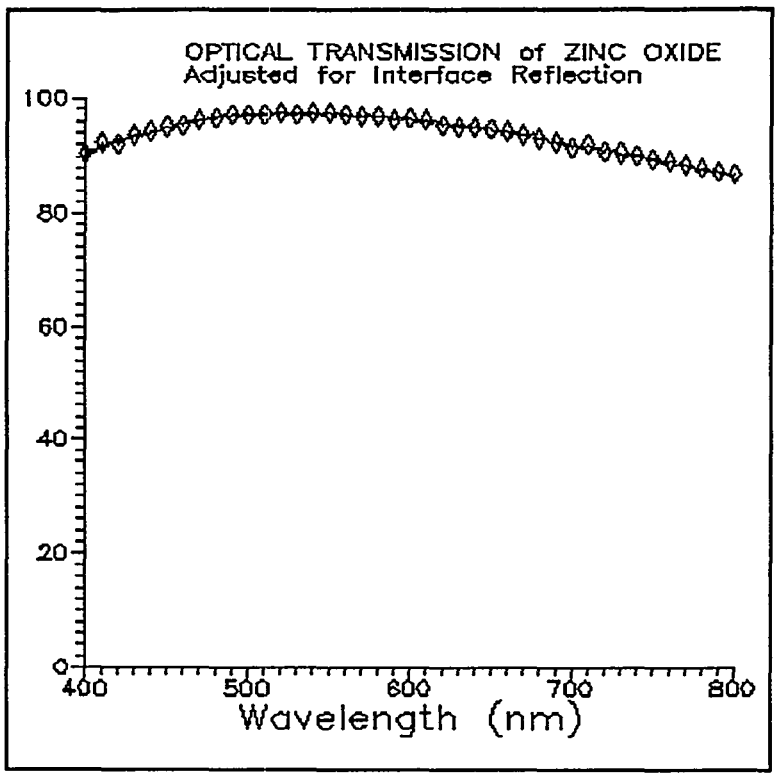

Figure 5.8. Optical transmission of reactively sputtered zinc oxide film after adjusting for interface reflections.

Figure 5.9 is a comparison of the quantum efficiencies measured on solar cells with an aluminum rear contact to the quantum efficiencies of solar cells with a reactively sputtered zinc oxide/aluminum rear contact. The short circuit current density of the solar cells with the zinc oxide/aluminum rear contact is an average of 9% higher than the short circuit current density of solar cells with the aluminum rear contact. A comparison of the photovoltaic parameters of these solar cells is given in **Table 5.3.** Although the short circuit current density is higher, the average fill factor of the devices with the reactively sputtered zinc oxide/aluminum rear contact is lower than that of the solar cells with aluminum. Further optimization of the zinc oxide deposition process is in progress.

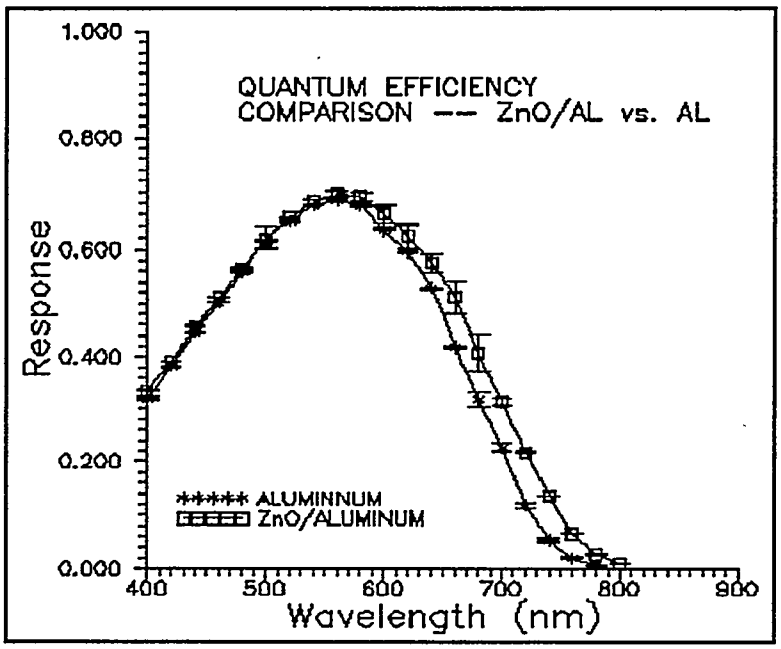

Figure 5.9. Comparison of quantum efficiencies for solar cells with aluminum rear contact to solar cells with reactively sputtered zinc oxide/aluminum rear contacts.

5.5 Comparison of Deposition Rates

One potential advantage of DC reactive sputtering from a metal target over RF sputtering from an oxide target is the significantly higher deposition rates of DC magnetron sputtering. Our current best RF sputtering process yields good quality zinc oxide films with a nominal thickness of 35 nm at a transport speed of eight linear inches per minute. In contrast, our best reactive sputtering process yields films with a nominal thickness of 100 nm at a transport speed of 10.9 linear inches per minute. The deposition rate achieved when reactively sputtering from a metal target is nearly four times the deposition rate achieved when sputtering from an oxide target.

REAR CONTACT	AVG. V_{oc} (Volts)	AVG. J_{sc} (mA/cm^2)	AVG. FILL FACTOR
ZnO/Aluminum	0.806 ± 0.004	12.04 ± 0.21	0.643 ± 0.006
Aluminum	0.816 ± 0.002	11.05 ± 0.04	0.703 ± 0.004

Table 5.3. Comparison of photovoltaic parameters of single-junction devices with different rear contacts. The zinc oxide was reactively sputtered in the large-area deposition system.

6.0 TASK 12: FRIT/BUS/WIRE/ENCAPSULATE/FRAME

6.1 Introduction

Efforts in this period were concentrated in three main areas. First, we have completed our development of a low cost, environmentally reliable connector for large-area photovoltaic modules. In a joint effort with a connector manufacturer, we developed and tested several connector designs leading to this final design. Currently we are continuing our work to develop or identify improved adhesive materials for connector mounting. Second, we have investigated alternative bus material formulations to address certain manufacturability constraints associated with large-area modules. Along with this material work, we have identified several equipment improvements that promise to provide better control of the dispensing process over large areas. Third, we have continued our efforts to develop low-cost encapsulants that will provide the environmental protection required and will enable the modules to pass environmental qualification tests. In this regard, we have developed two classes of encapsulation materials that enable us to pass the wet high potential test. As part of our encapsulation development, we have begun to investigate the utility of insulating films in combination with these encapsulation materials.

Work on automated testing of wiring, sealing and encapsulation has been postponed pending the investigation of alternative application methods for encapsulant and the connector housing. We have begun to investigate frameless module concepts on a limited basis; however, we have postponed significant effort in this area until we have better specified our encapsulation scheme.

6.2 Module Electrical Connector

In this period we have participated in a joint effort with a connector manufacturer to develop a low-cost, environmentally sound connector for large-area modules. The complete connector assembly consists of a tab connector that electrically connects the module to the module lead wire, and a housing that provides mechanical support and environmental protection. The connector assembly must meet several requirements for photovoltaic module applications. The connector must provide a reliable, low resistance electrical connection between the module and the module lead wire. It must withstand both the pull and torque stresses that are likely to be encountered during module assembly and field installation and must meet manufacturability standards. In addition, the electrical and mechanical integrity of the connector must not be compromised by exposure to the environment.

Several connector designs and connector mounting materials were evaluated in this period. Prototype connectors supplied by the manufacturer were subjected to a series of tests designed to measure the mechanical and electrical reliability of the connector. The tests included pull strength measurements, torque strength measurements, thermal cycling, and insolation resistance tests. After each round of tests, the results were reviewed with the connector manufacturer. Based on the test results, the connector design was modified and again tested to determine the effect of the modification. Using this process, the design of both the tab and the housing were modified.

The major modification made to the tab was to increase the dimensions of the tab base. The effect of this modification is summarized in **Figure 6.1.** This figure shows a comparison of pull strength measurements made on the original tab and revised tab. The average pull strength measured on the original tab was approximately 164 N (37 lb.). The average pull strength measured on a revised tab, rose to 249 N (56 lb.).

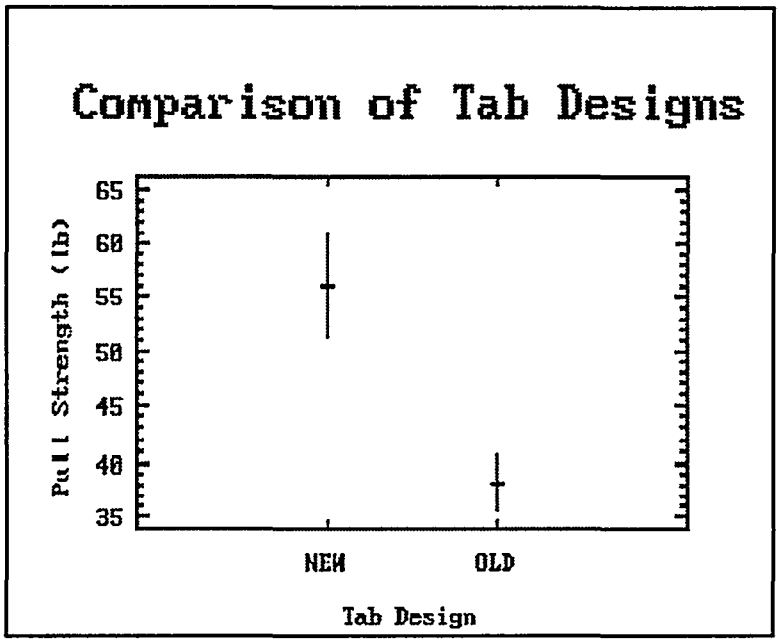

Figure 6.1. The horizontal lines show the average of the pull strengths for each group. The vertical lines indicate the standard error of measure for each group.

The effect of bonding area on the average pull strength of a tab was also investigated. The tab bonding area is determined in part by the width of the bus. **Figure 6.2** is a comparison of the pull strengths measured for tabs bonded to bus material of three different line widths. As indicated in **Figure 6.2,** a 60% increase in bus line width resulted in a 98% increase in pull strength. In addition to initial pull strength, the effect of thermal cycling on tab pull strength was investigated. A comparison of tab pull strengths before and after 50 thermal cycles, is shown in **Figure 6.3.** A statistical test of significance indicates there is no detectable difference between the average tab pull strengths before and after 50 thermal cycles.

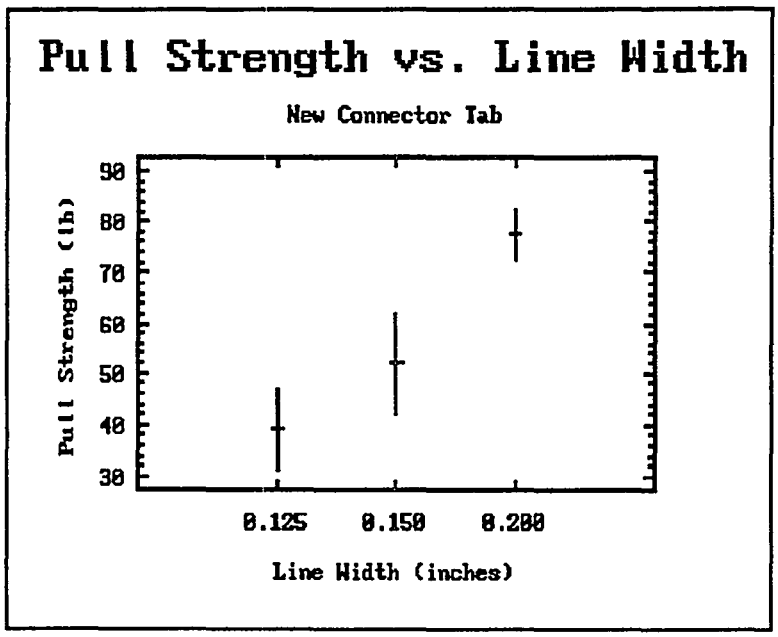

Figure 6.2. The effect of bus line width on tab pull strength. The horizontal lines indicate the average of the pull strengths for each group. The vertical lines indicate the standard error of measure for each group.

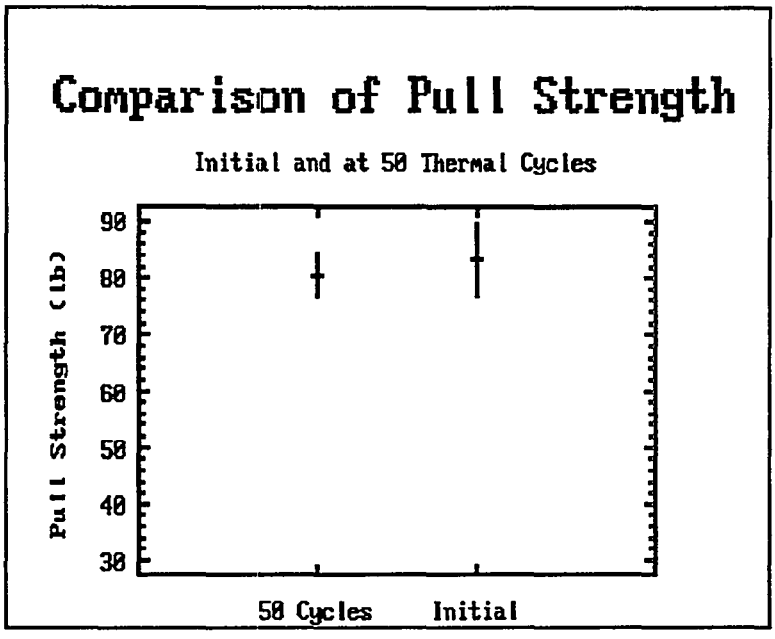

Figure 6.3. The effect of 50 thermal cycles on tab pull strength. The horizontal lines indicate the average of the pull strengths for each group. The vertical lines indicate the standard error of measure for each group. There is no statistically significant difference in the average pull strengths.

The housing of the connector was also modified. The connector housing is mounted on a module with an adhesive material. Several types of adhesives were evaluated for this application including flexible epoxies, chip adhesives, two component epoxies and cyanocryalates. Based on a recommendation of the connector manufacturer, a fifty-pound pull test was used to screen potential housing adhesives. One class of adhesives, the two component epoxies, was found to provide the required pull strength. Of the housing/adhesive combinations that failed this test, the failures occurred primarily at the interface between the housing and the adhesive, suggesting that this interface was generally weaker than the adhesive/encapsulant interface. Based on this result, several attempts have been made to increase the strength of this interface by modifying the surface of the housing base. These modifications included priming, micro blasting and mechanical roughening. The result of these surface modifications has been inconclusive.

An alternative approach to increase the strength of the adhesive/housing interface has been to vary the mix ratio of the two components of the epoxy. A summary of the results obtained by varying the ratio of the two components from 1:3 to 1:4 is given in **Figure 6.4.** As the ratio of the two components was changed from 1:3 to 1:4, the connector pull strength decreased from 325 N (73 lb.) to about 60 N (13.5 lb.). There is some evidence to suggest that there is a mismatch between the thermal expansion properties of the epoxy mixture and the module. Experiments changing the volume of adhesives applied to the housing, and changing the mix ratio of the components will be continued.

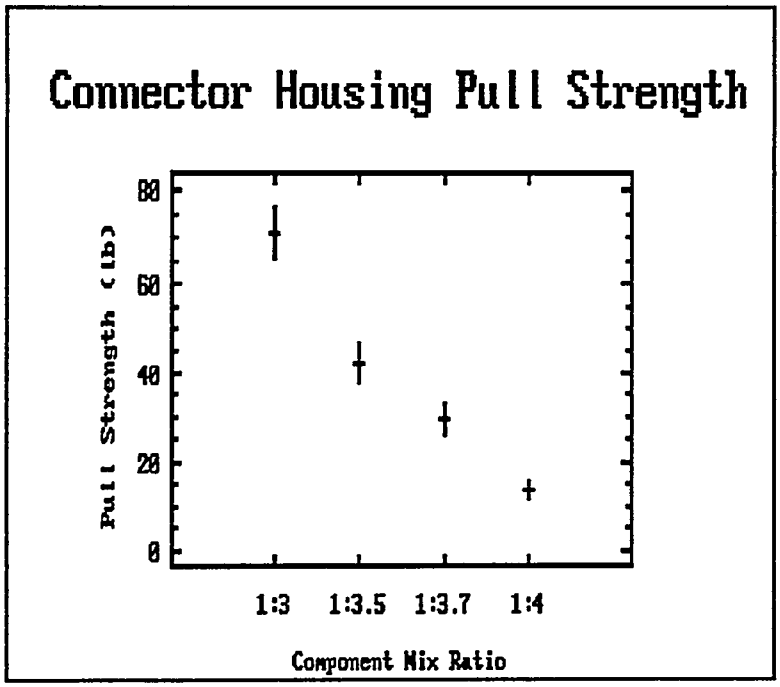

Figure 6.4. The effect of adhesive component mix ratio on the connector housing pull strength. The horizontal lines indicate the average of the pull strengths for each group. The vertical lines indicate the standard error of measure for each group.

The modifications made to the connector tab and housing have greatly improved the utility of the connector for large-area photovoltaic module applications. These modifications have resulted in a significant increase in the pull strength of the tab. In addition, the larger size bases of the tab and housing will facilitate mounting the connector assembly on the module, improving manufacturability of the connector assembly. We plan to continue our evaluation of different adhesive materials.

6.3 Bus Material Evaluation

Scaling-up the bus dispensing, drying and curing processes to large-areas presents several unique challenges. As the size of the module substrate is increased, the bus material is dispensed over longer distances. Consequently, the locational tolerances that must be held in the dispensing process become correspondingly tighter. In addition, the flow of material must be kept uniform over these relatively long distances to achieve a bus with constant line width and uniform cure characteristics throughout the length of the bus. These constraints place tight demands on the mechanical alignment of the large-area dispensing system, the dispensing valve mechanism, the material delivery system and the firing process. The physical properties of the bus material must be well controlled to maintain good control of the processing steps.

In the previous period we designed and constructed a large-area bus dispense station that is capable of maintaining the required mechanical tolerances. In this period, we have concentrated on addressing the manufacturability issues associated with scaling-up the bus dispense and firing processes. First, we have evaluated alternative bus material formulations to relieve some constraints associated with the material properties. Second, we have identified a material delivery system that has the potential of yielding significantly better control of the dispense process. Better control of the dispense process will translate directly into better control of the drying and firing processes.

Our standard bus material formulation gives good line width control and excellent pull strengths both before and after environmental stress tests. To widen the window of acceptability of the bus dispense and firing processes, we evaluated several alternative formulations of the bus material. Our standard bus formulation was used as a baseline for evaluating these alternative formulations.

The dispensing and firing characteristics of bus material depend on several physical characteristics of the material including, the viscosity of the material, the fractional

percentage of solids in the material and the ratio of the component mix. Accordingly, we evaluated several formulations with different fractional percents of solids and component mix ratios. In one study, the fractional percentage of solids was increased to determine the effect of a higher density of solids on the dispensing and firing characteristics. The dispense characteristics of this formulation were good. We achieved line width control comparable to our standard formulation. The initial pull strengths measured on this formulation were also good, ranging from 169 to 182 N (38-41 lb.) which is again comparable to our standard formulation. During thermal cycling, however, stress fractures occurred in a small percentage of the solder joints. Analysis suggested that a mismatch in thermal expansion between this high density bus formulation and the glass substrate, caused these stress fractures. Several modifications to this high density formulation were investigated. These modifications involved changing the mix ratio of the solid components in the bus material while maintaining the relatively high density of solids in the mix. A comparison of the pull strengths measured on one alternative formulation with the pull strengths typical of our standard formulation is shown in **Figure 6.5.** Although we have identified several promising alternative formulations, to date, we have not identified a formulation that is superior to our standard bus material. We plan to evaluate several newer formulations soon.

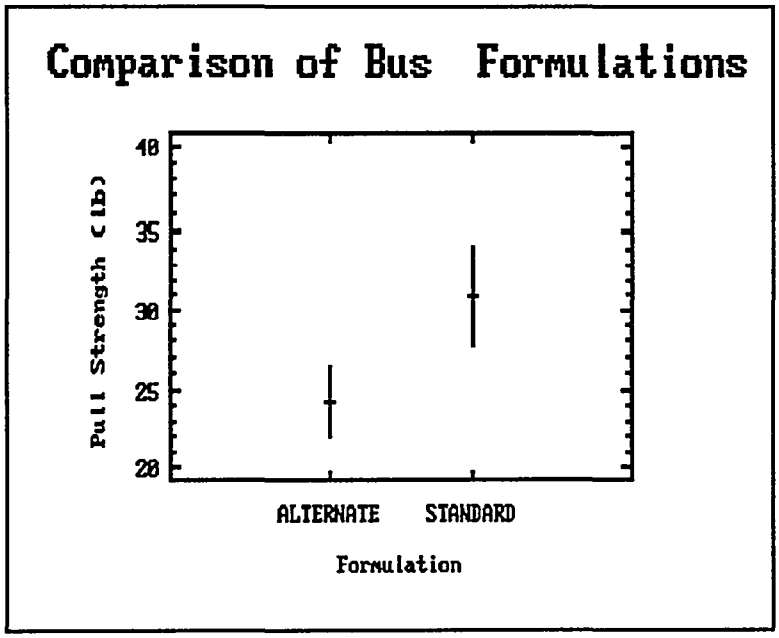

Figure 6.5. Comparison of the pull strengths measured on standard bus material formulation to the pull strengths of an experimental formulation. The horizontal lines indicate the average of the pull strengths for each group. The vertical lines indicate the standard error of measure for each group.

An alternative bus material is one approach to easing the strict process control required in large-area bus deposition and firing. Besides changing the starting material formulation, recently, we have investigated alternatives to our current delivery system. Our current system is based upon a time and pressure relationship to control the amount of bus material per unit length to the module. Although the system works well for large-area substrates, the inherent variation in this system forces certain compromises in the subsequent firing process. We are now investigating the possible advantages of a positive displacement pumping system to control the amount of material dispensed on a substrate. The compatibility of the bus material and this new pumping system has been verified. In this next period we plan to perform a full evaluation of this delivery system.

6.4 Encapsulation Development

Large-area modules intended for use in photovoltaic systems must be encapsulated not only to protect the module, but also to protect installation and service personnel from accidental exposure to the high electrical voltages that are present in a photovoltaic system. In a previous period, we evaluated several different encapsulation materials by subjecting samples of these materials to a series of screening tests. These screening tests included: water immersion (per Solarex internal specification), a cut test (per UL 1703 specification), UV exposure, thermal cycling, humidity-freeze and wet high potential. The last three tests were performed according to the procedures outlined in the SERI/TR-213-3624 document. A summary of the wet high potential test results is presented in **Figure 6.6.** Three different materials groups were investigated: UV curables, polyester urethanes and acrylic urethanes. Of these, the best results were obtained with the acrylic urethanes applied using a multi-coat spray process.

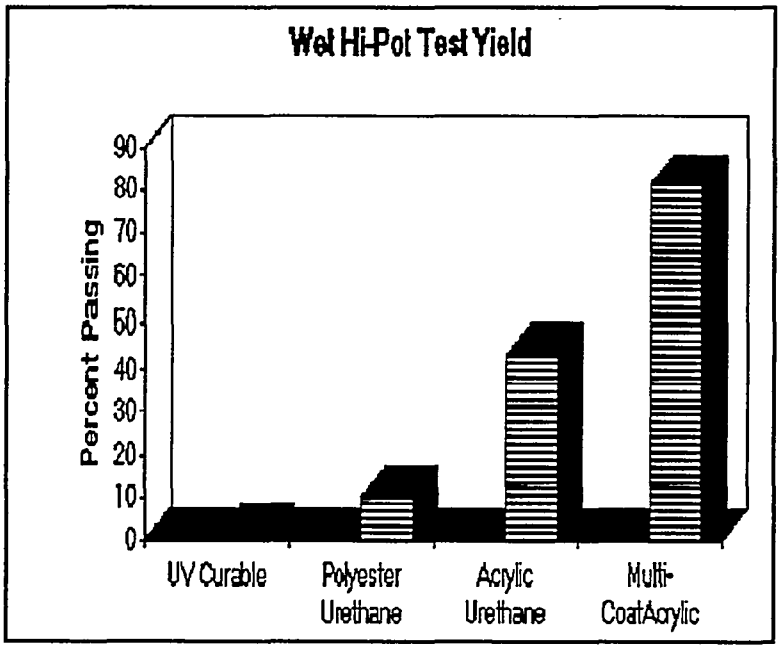

Figure 6.6. Summary of wet high potential test yields for various encapsulant materials. The test voltage was 2250 volts.

The acrylic urethane materials showed the highest potential for obtaining 100% yield on wet high potential tests, however, there are several disadvantages associated with using these materials. Since these materials have a high solvent content, the encapsulant requires specialized drying equipment suitable for handling the solvent effluents. In large quantities, this effluent handling equipment represents a significant capital investment. In addition, the material transfer rates are relatively low, further complicating waste handling. These materials are multi-component systems and after mixing the separate components, the mixed material has a limited pot life. Finally, the maintenance of multi-component encapsulant delivery systems is more complicated than it is for single-component delivery systems.

As an alternative to acrylic urethane materials, we have developed a UV curable formulations to use as a photovoltaic module encapsulant. UV curable encapsulants address all of the issues associated with the acrylic urethanes and are, therefore, potentially more cost effective. The improvements we have made in our UV curable encapsulation are summarized in **Figure 6.7.** The yield of wet high potential testing to 2250 volts has risen from essentially 0 to over 64%. After 50 thermal cycles, the wet high potential testing yield to this same test voltage is about 71%.

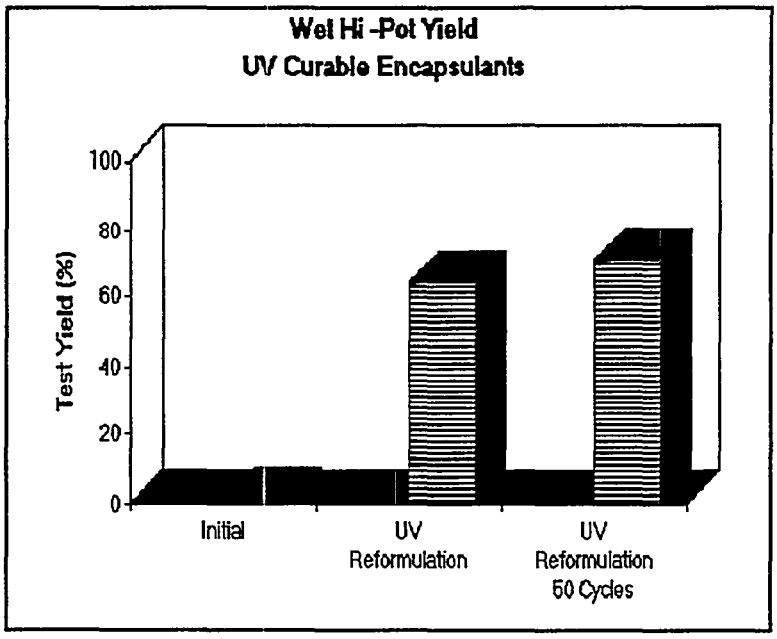

Figure 6.7. Wet high potential test yields for UV curable encapsulants before and after 50 thermal cycles.

Examination of the plates that failed the wet high potential test suggests that the primary cause of failure is debris trapped inside the encapsulant leading to pinhole defects in the encapsulant. This was found to be the case for both the UV curable encapsulants and the multi-coat acrylic encapsulants. We are currently investigating several methods to eliminate these defects including improved cleaning and surface preparation procedures and alternative application methods. We plan to continue our development efforts with both the UV curable and the acrylic-based materials.

Recently, we have begun to investigate the utility of using insulating films such as tefzel in combination with the encapsulant materials to improve the wet high potential test yield. The preliminary screening tests of these combination encapsulant schemes are now underway. Preliminary results are promising. The modules held up extremely well in several screening tests.

7.0 TASK 13: MATERIALS HANDLING

7.1 Introduction

In this period, we have continued to develop a 10 megawatt (MW) per year capacity production facility layout. Several issues related to glass handling, raw materials storage and finished good storage in a 10 megawatt production facility have been addressed. In the area

of glass handling, we have examined two alternatives, incoming glass cut to size and incoming glass that is uncut. We have identified commercially available glass handling equipment that will be used to handle fully encapsulated modules and also raw glass. In addition to glass handling issues, we have identified the receiving and storage issues related to the other raw materials that are required to fabricate modules.

A complete production facility layout must provide for quality control plans, line maintenance and line support. In this period, we have begun to incorporate these functions into our facility layout.

7.2 Plant Layout Design Process Flow

In the last reporting period we considered a layout of the production equipment with a projected output capacity of 10 megawatts. In this period we expanded our analysis to include, glass handling equipment, integration of this equipment with the module production equipment, raw material storage and inventory management, and management of product inventories. A flow diagram of our plant layout design process is shown in **Figure 7.1.** This figure outlines the process that was followed in developing a plant layout.

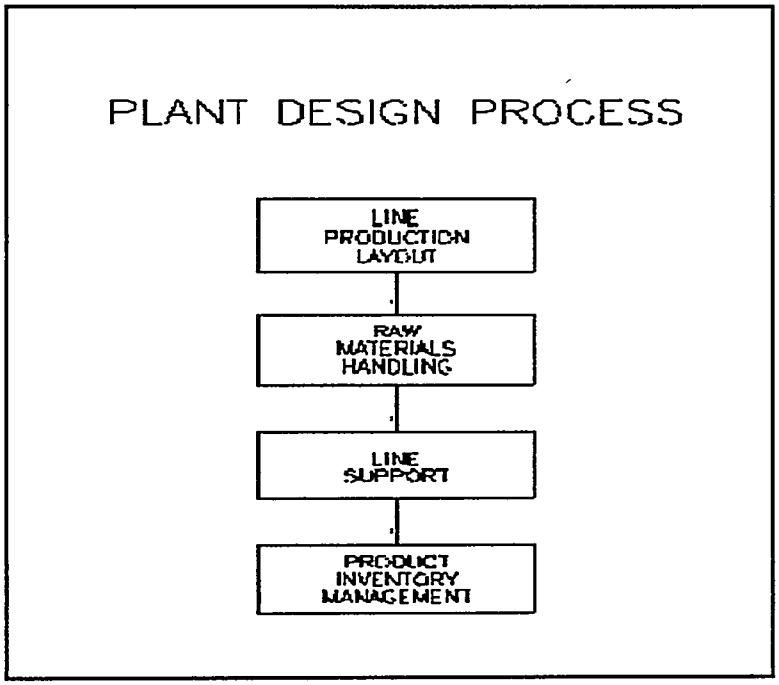

Figure 7.1. Plant Design Process

The first step in this process was to sketch the module fabrication line layout. The various types of plant layouts were examined to determine which of these layout approaches best

suited our approach to module fabrication. After determining the basic design approach, several detailed designs were considered. To choose one detailed design, material handling issues were examined. For our purpose, material handling included receiving and storage of raw material and moving this raw material onto the production line. Based on an examination of how raw materials would be moved, a module fabrication line design was chosen to efficiently move material throughout the plant. The third phase of our plant design process was to consider the line support functions which include quality assurance activities and line maintenance activities. Quality assurance activities occur during all of the stages of the production process: at raw materials receiving, various points in the production line and at final product packaging. Line maintenance activities may occur at any point along the line as well as off line.

A complete plant layout design would also consider final product inventory management and the location of plant facilities. A final product inventory management approach has been chosen, however since some of the module finishing processes are still under development, we have not completed this phase of our plant layout. In addition, we have not completed our analysis of plant facilities yet.

The actual path to developing a plant layout was more complicated than is outlined in **Figure 7.1.** Since at each step in the design process considerations may arise that impact earlier steps, the actual design process was iterative. The process outlined in **Figure 7.1** is intended to provide an idea of the scope of the plant layout considered herein. Implicit in the design process is the consideration of inventory management and control systems such as Just-In-Time (JIT) and Materials Requirements Planning (MRP).

7.3 Line Production Layout

There are three general types of plant arrangements. In a layout by fixed position material location is fixed and the tools and subassemblies used to build up the completed product are moved to the location of the major assembly. This type of layout is appropriate for complex products which consist of many subassemblies. The second type of layout is a layout by function or process. In this type of layout, operations of the same process are grouped together and the material is moved sequentially from one process step to the next. The third major type of plant layout is a layout by product. In this type of layout, the material is also moved sequentially from one process to the next. In contrast to the layout by function, the equipment used to make the product is arranged according to the sequence of operations. A layout by fixed position is clearly not appropriate for module fabrication. A layout by function would be more appropriate to a batch mode of operation where

machines performing the same process step are grouped together in the same area, and different process steps are located at separate stations. Since we envision an integrated line for module fabrication, the basic layout approach is that of a continuous line or a layout by product.

The basic line production layout for a 10 megawatt per year capacity plant is shown in **Figure 7.2.** Material is moved from one process step to the next in a continuous line. This type of approach is ideally suited to production situations where there is a large quantity of pieces to be made and where the design of the product is fairly standardized. A unique requirement of this layout approach is that the flow of material be balanced throughout the line. For this reason, attaining a balanced flow of material throughput is an important process development consideration.

The layout shown in **Figure 7.2** covers all of the module fabrication steps from glass seaming through encapsulation. The module finishing steps which include connector mounting and framing will be done on a separate integrated line. The two lines will operate independently, each with a distinct balance. This feature adds flexibility to the entire process by allowing customization of features at the module finishing stage to meet specific customer requirements. Since each line can be viewed as having separate functions, one module fabrication and the other module finishing, the 10 megawatt per year capacity plant layout is actually a hybrid of the layout by product and the layout by function.

This overall plant layout offers several unique advantages. First, although balance must be maintained within each line, it need not be maintained from one line to the other. This provides flexibility in work scheduling, product customization and maintenance scheduling. Second, it avoids the necessity of balancing vacuum deposition processes to the module finishing processes. Third, separating the module fabrication processes from the module finishing processes provides a means for optimizing material inventory management and control systems to each line and to the overall plant output.

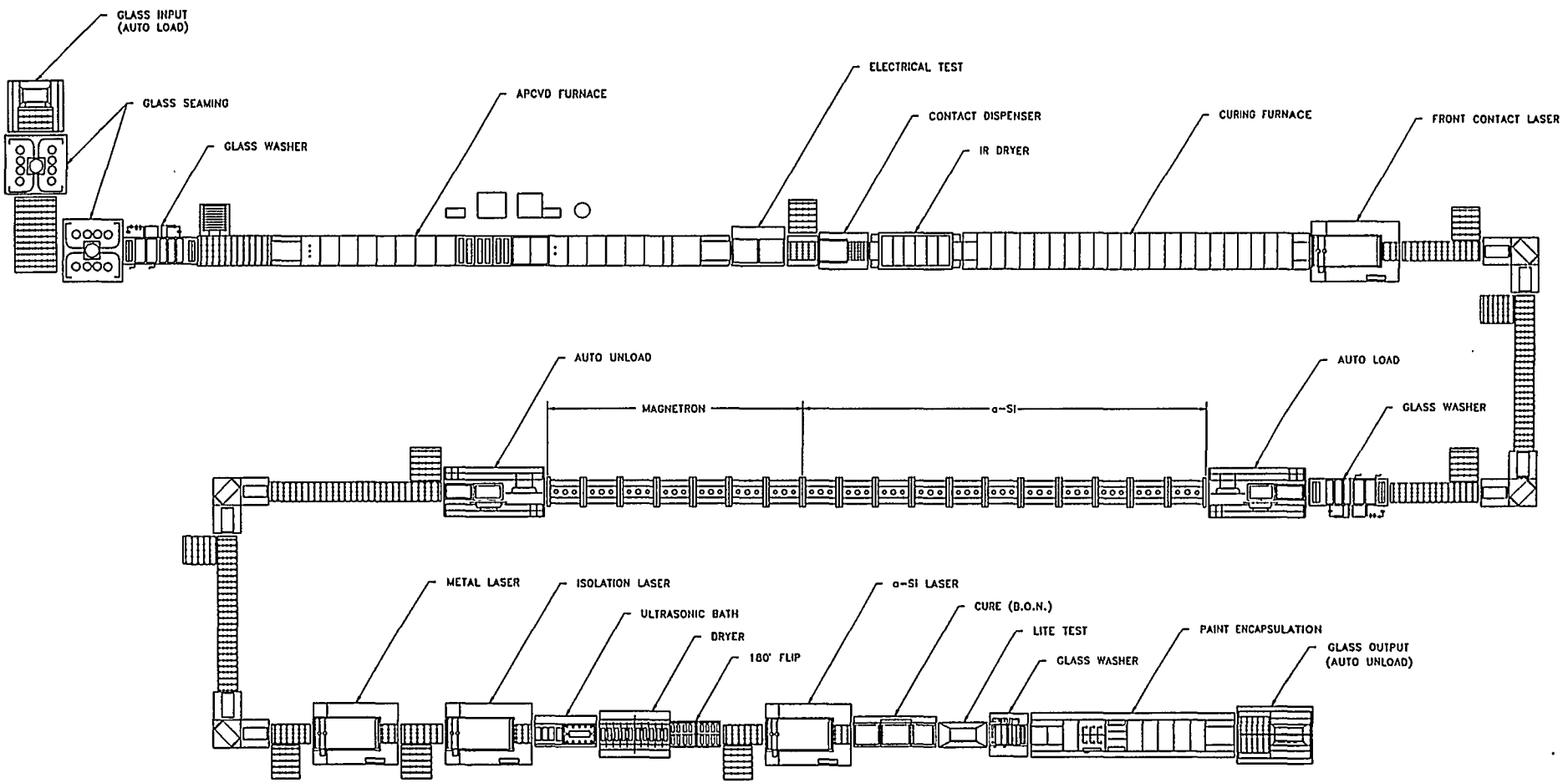

Figure 7.2. Ten megawatt module line layout. The layouts for the raw glass area and the final product area are not shown.

7.4 Raw Materials Handling

To adequately plan for raw materials handling and control systems, several items must be considered. These include quality assurance procedures, safe storage and handling procedures, inventory planning and control systems, and the movement of material to the point of use. As a first step to planning for materials handling, the materials that are used to fabricate completed product were assigned to one of several classifications based upon the type of material and any special handling requirements. These classifications were glass, compressed gases, liquid chemicals, finishing materials and general stock items. The first three classes of materials require specialized handling and storage techniques. These techniques must be integrated into the plant-wide raw materials and control system.

7.4.1 Glass Handling

The specific glass handling procedures and equipment that will be used in the 10 MW per year capacity plant will depend upon the degree to which the glass is finished upon receipt at the plant. Two scenarios were considered. In the first scenario, glass is received from the glass manufacturer precut and ready for the seaming process. In the second scenario, raw glass is received in large sheets and cut to the required size in-house prior to seaming.

Figure 7.3 is a schematic diagram of a cut glass inventory area. This figure illustrates the flow of cut glass from the receiving dock to the module production line. Glass is received on reusable glass racks. These same racks are used to store and transport raw glass in the plant. The glass will be stacked in a near vertical position on the glass racks and a commercially available automated glass unstacker will be used to remove the glass from the glass rack. The glass unstacker will orient the glass horizontally and place it onto a glass load station. The glass load station will index the glass and automatically load it onto the edge seamer. The glass racks, the glass unstacker and the glass seamer are all commercially available and can be purchased from several manufacturers. The only requirements that must be met to integrate this glass handling equipment into the module production line is to integrate the glass seamer into the line and properly time the sequence of glass unstacking and movement. Based on our experience with our existing integrated line, these requirements should not be difficult.

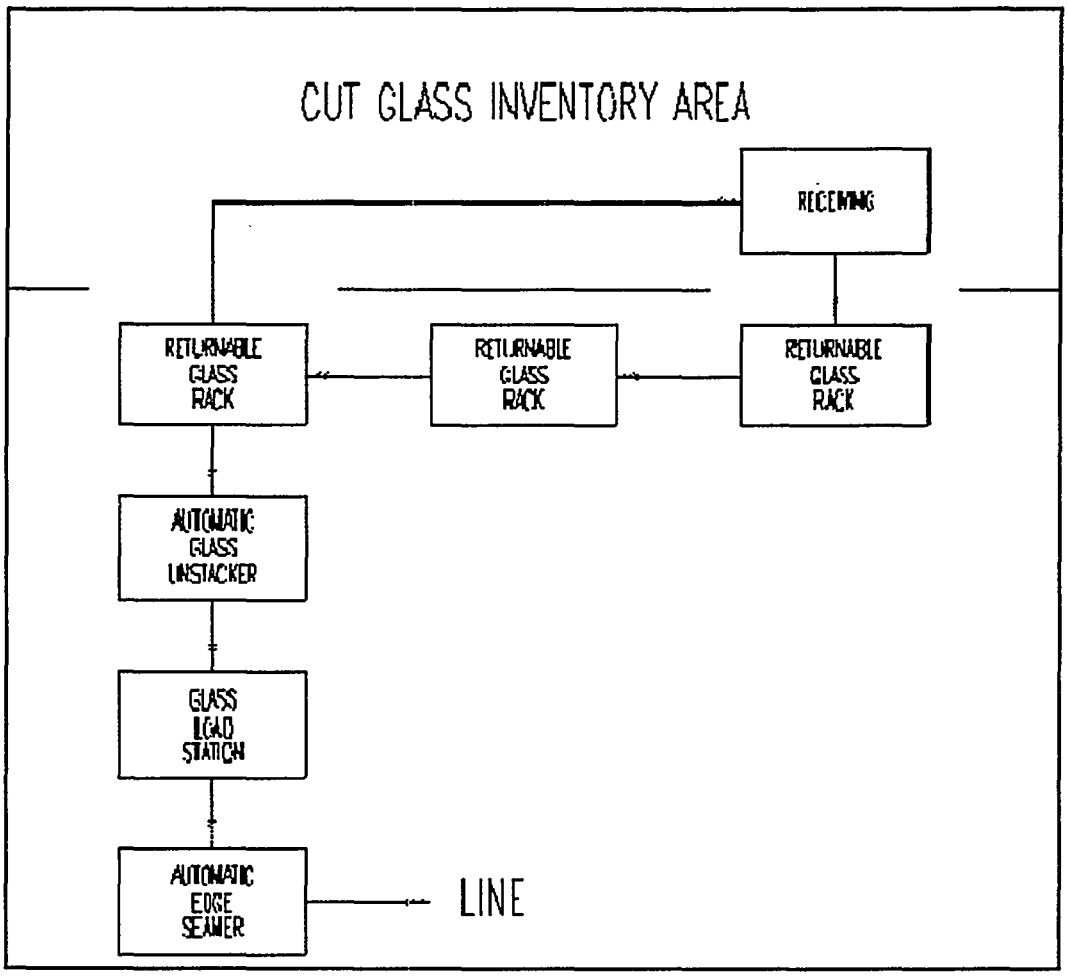

Figure 7.3. Layout of the cut glass inventory area. This area is located at the front of the module production line.

An alternative to receiving cut glass is to install the capability to handle large sheets of glass and cut them to size. **Figure 7.4** is a schematic diagram of an uncut glass inventory area located at the front of the module production line. As in the case of precut glass, uncut glass will be received from the glass producer on returnable glass racks. The automatic glass unstacker will remove glass a single lite at a time, orient it in a horizontal position and place the glass onto an automated glass cutter. After indexing, the glass will be scored to the proper dimensions at the glass cutter and then transported on a series of rollers to an air float breakout table where the glass is broken into the proper size. Any waste glass will be collected off to the side of the breakout table for disposal. The cut glass will be automatically transported to the glass load station where it is indexed and loaded onto the glass seamer. As in the previous case, all of the glass handling equipment is commercially available and should be easily integrated into the module fabrication line.

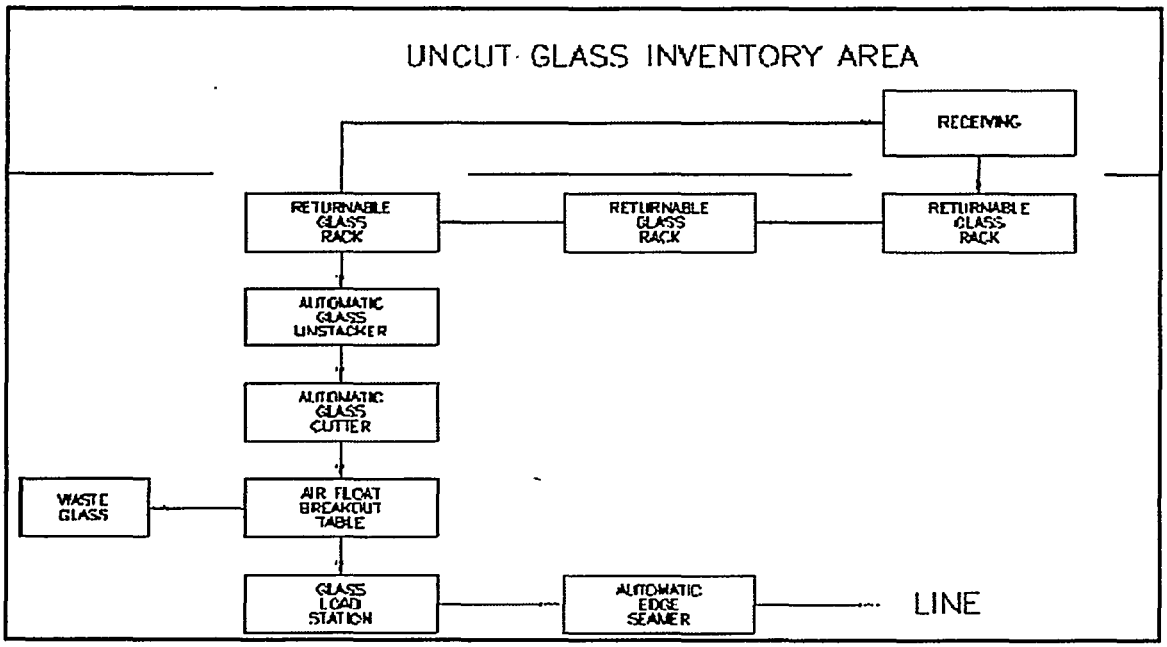

Figure 7.4. Layout of the uncut glass inventory area. This area is located at the front of the module production line.

Quality assurance activities in the glass inventory area will be limited to a visual inspection of the glass on the glass rack to verify no damage has occurred in shipment. For safety reasons, glass handling will be fully automated at the front of the production line.

The scenarios described above have several advantages. First, the number of times that the raw glass is physically moved and the distances over which the glass is moved, are minimized. Raw glass is received and moved directly to the production area at the point of use. This reduces the safety hazards associated with glass handling. Second, the transactions from receiving to stock and from stock to the line are eliminated, thus simplifying inventory control.

7.4.2 Compressed Gas Handling

Compressed gases are used at various stages throughout the module production line. Due to the nature of these materials, several precautions must be observed to safely handle and store compressed gas cylinders. In addition, any materials control system for compressed gases must conform to the Occupational Safety and Health Administration (OSHA) regulation 29 CFR 1910.166-171. A schematic diagram of the area for storing compressed gases is shown in **Figure 7.5.** This storage area will be located near a separate receiving area and, as with raw glass, the gas cylinders will be received directly into stock. This area will be specifically designated for storage of compressed gas cylinders. Within the storage

area, gases will be segregated by hazard category and clearly marked. Empty cylinders will also be stored in this area. This area will be fully outfitted with gas monitoring and safety systems. For safety reasons, the gas cylinders will be located in an area that is removed from the main operational and facilities areas of the plant. The cylinders will be transported to the point of use on an as-needed basis.

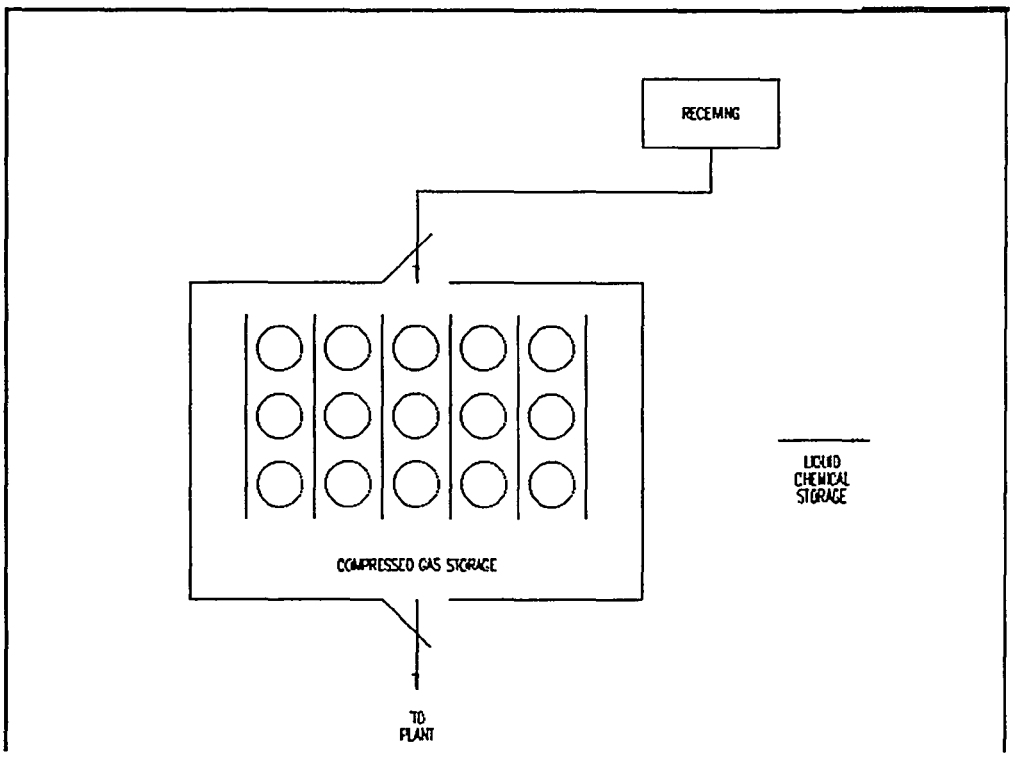

Figure 7.5. Layout of compressed gas storage area.

This system of storage offers several advantages. First, the number of times the compressed gas cylinders are moved is minimized. Minimizing the number of times compressed gas cylinders are moved helps to mitigate the hazards associated with transporting gas cylinders. Second, the arrangement of gas cylinders outlined promotes first-in/first-out stock rotation.

7.4.3 Liquid Chemical Storage

The volume of liquid chemicals used to fabricate large-area modules is relatively small. Nevertheless, since they are used, special provisions are required to handle and store the chemicals safely. The plant layout for liquid chemical storage must conform to OSHA regulation 29 CFR 1910.106 and the National Fire Protection Association (NFPA) Standard number 30.4310. For example, this room must be constructed of materials having at least a two-hour fire resistance rating, with self-closing Class B fire doors.

7.5 Inventory Control Systems

The integration of the module fabrication processes into a continuous line, forces tight control of the work-in-process (WIP) inventory. This tight control of work-in-process is characteristic of JIT inventory management systems. There are several advantages to extending the JIT inventory control system to include raw material inventories. First, raw material inventories are kept low. In the case of materials such as glass, compressed gases, and liquid chemicals, low inventory quantities mitigate some of the hazards associated with these materials. Second, the total area designated for storage in the plant is minimized. This is particularly advantageous if the storage area requires special preparation, as in the case of a liquid chemical storage room. Third, JIT promotes partnership arrangements with suppliers thereby reducing costs and raising quality. Finally, JIT promotes continuous improvement throughout plant operations by uncovering any weaknesses in line. For these reasons, we have designed this layout assuming a JIT system of inventory control.

7.6 Product Inventory Management

Figure 7.6 is a schematic diagram of the final product inventory area for the 10 MW plant. Since the specific module finishing processes are still being defined, we have not fully investigated automated packaging equipment for large-area modules. The automated packaging equipment shown in **Figure 7.6** is a conceptualization based on our current product design. As the finishing processes are further defined, we intend to better define this layout.

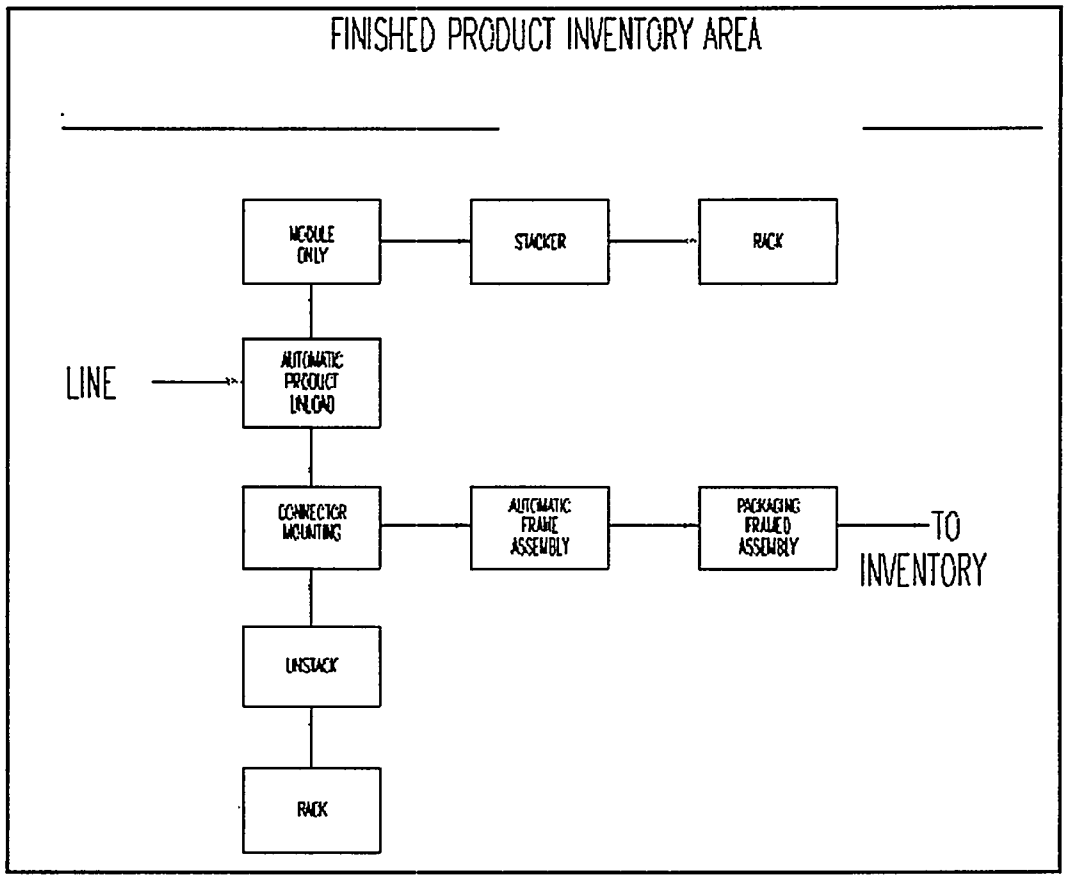

Figure 7.6. Conceptual drawing of the finished product inventory area.

Fully encapsulated modules will enter the final product inventory area and be routed in one of two directions. Modules that are not scheduled to be finished immediately will be off loaded onto a glass stacker system, which will stack the modules onto a portable glass rack. These systems are similar to those used for handling raw glass. Alternatively, modules to be finished will be off loaded and routed to an automated module finishing line. Once the finishing steps are completed, the modules will be packaged and either placed in stock or shipped to the customer. To finish the modules stored on the glass storage racks, the racks can be moved to a glass unstacker system where the modules are loaded onto the module finishing line.

The final product inventory area shown in **Figure 7.6** has several advantages. First, the finished goods inventory is kept low. Modules can be finished as required to replenish stock or meet a customer order. Second, it allows the flexibility to customize the finishing process without maintaining a large inventory of product variations. Finally, the module production line and module finishing line can be balanced independently.

8.0 TASK 14: ENVIRONMENTAL TEST, YIELD, AND PERFORMANCE ANALYSIS

8.1 Introduction

In this period, efforts were concentrated in three areas. First, we have designed, built, and tested an automated cure station to burn out electrical defects in large-area modules. This curing system can accommodate substrates up to 0.61 m (24 in) wide by 1.83 m (72 in) long. Second, we have continued our indoor and outdoor testing of prototype modules. Test modules range in size from 0.101 m^2 (1.08 ft^2) to 0.37 m^2 (4 ft^2). Indoor and outdoor environmental tests have been used to evaluate materials of construction, fabrication processes and module design concepts. Third, we have performed an initial yield study which will lead to a more comprehensive process control study. In this yield study we have tracked the yield at each of the major module fabrication steps and used the results of this study along with our high potential yield and performance yield to estimate an overall line yield.

8.2 Large-Area Cure Station

Pinhole defects that occur during the fabrication of thin film multi-junction solar cells may act as a low resistance current path reducing the shunt resistance of the cell. If these electrical shunts are large enough, they will adversely impact the performance of the solar cell. As photovoltaic modules become larger, with correspondingly larger segment areas, the effect of these electrical defects is cumulative so as to seriously degrade the performance of the module. These defects can be removed however by applying a sufficiently large reverse voltage to the segments, to burn out the defects. To automate this electrical cure process we have designed, built and tested a large-area electrical cure station.

This electrical cure station is capable of accommodating substrates with dimensions up to 0.61 m (24 in) by 1.83 m (72 in). A schematic diagram of the station is given in **Figure 8.1.** The main components of the cure station are the module support bed, the cure head, the electronic control system and the display panel. The support bed is constructed of a series of rollers to facilitate module loading and unloading and to support the module evenly during the cure process. The cure head contains a series of pins that make electrical contact to the module. These pins are arranged in a pattern that corresponds to the segment pattern of the module. After the module that is to be cured is loaded, the cure head is lowered to bring the pins in contact with the module segments. The control unit positions the cure head and controls the entire curing process. This unit can be programmed to change any of the cure parameters. The status of each segment cure is displayed on the

display panel in real time. In addition, an RS232 port provides the capability to remotely monitor the cure process for central data collection and analysis.

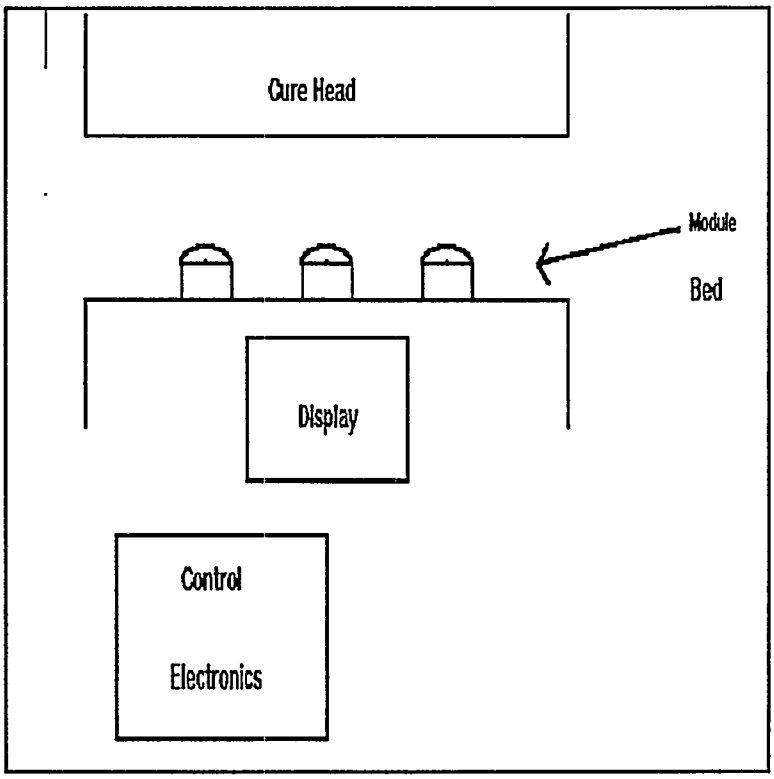

Figure 8.1. Schematic diagram of the large-area cure station.

Figure 8.2 is a bar chart of the normalized output power of 0.37 m^2 (4 ft^2) modules before and after electrical cure on the large-area cure station. Before cure, the average normalized output power of the modules was 84.1% of the maximum value. After the automatic cure, the average normalized power was 100%. A manual cure was performed on these modules after the automatic cure to verify that the electrical cure performed by the cure station was complete. The output of the modules was unchanged before and after the manual cure, indicating that the automatic cure station completely cured the module.

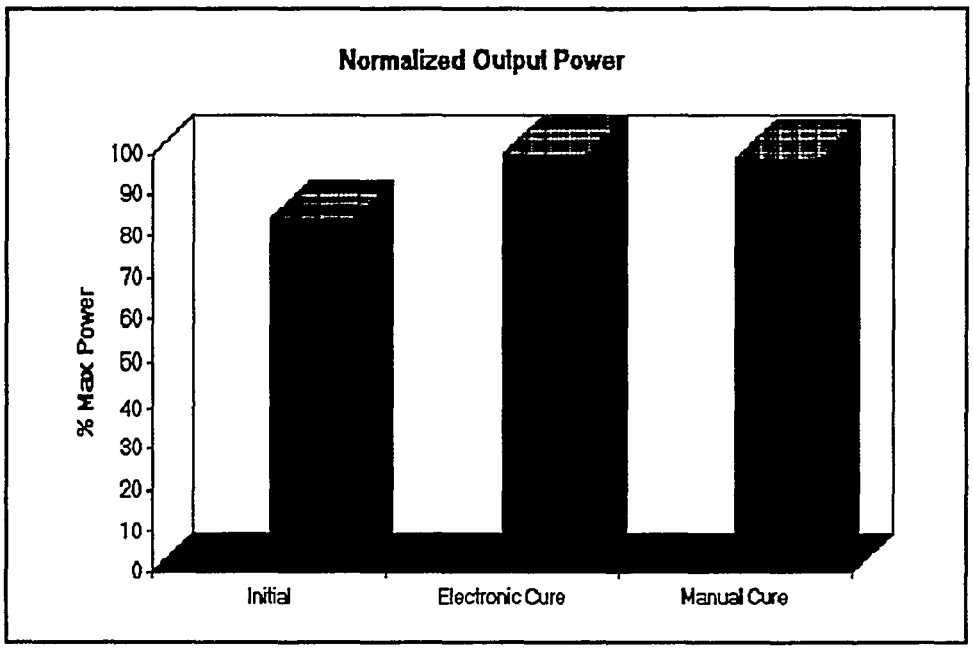

Figure 8.2. Comparison of normalized module output power before automatic cure, after automatic cure and after a manual cure. The manual cure was done to verify that the automatic cure process is optimum.

8.3 Environmental Testing

In the previous period, we expanded our indoor environmental testing capabilities to accommodate module sizes up to 0.56 m^2 (6 ft^2). Most of the equipment and procedures that are required to perform the tests outlined in the NREL Interim Qualification Test document (SERI/TR-213-3624) have been installed. In this period, we have used this testing capability to evaluate a number of candidate materials and methods of construction for fabricating large-area modules. In addition to these indoor tests, we have installed the capability of performing the Field Wet Resistance Test (FWRT).

Environmental testing is an essential element of our process development and product development work. We routinely use specific tests or specific test sequences to evaluate alternative fabrication processes, alternative materials and alternative methods of constructing large-area modules. Test modules may range in size from 0.101 m^2 (1.08 ft^2) to 0.37 m^2 (4 ft^2). The most difficult test has been the wet high potential test. The results of our indoor testing and our progress to date are discussed in Section 6.0 of this report.

In addition to indoor testing, in this period we have also carried out an extensive outdoor exposure study. The purpose of this study was to investigate a total of nine factors related to module fabrication. A list of these factors is given in **Table 8.1.** The first eight of these

factors (factors A through H) were each set at one of two levels corresponding to one of two alternative materials or processes. The ninth factor was set at one of three levels, corresponding to one of three test configurations. To test these factors, multi-junction modules were constructed using different combinations of materials and processes. The specific combinations of factors A through H that were used to construct these modules were determined from a 1/16th fraction, 2-level, 8-factor experimental design. These combinations of factors are shown in **Table 8.2.** In this table the two unique values of each of eight factors are represented by a + or - sign. For example, factor D - encapsulation type refers to one of two encapsulation materials that were tested. The + level of this factor is an acrylic-based material and the - level is a polyester-based material. There are 16 unique combinations of eight factors shown in **Table 8.2,** each combination represents one module. To compare mounting configurations, 16 modules were fabricated for each of the mounting configurations. A total of 48 experimental multi-junction modules, plus 16 control modules, were deployed.

Prior to deploying the test modules, each module was electrically tested, visually inspected, and subjected to a 2250 vdc dry high potential test, a 1000 vdc wet high potential test and a 500 vdc wet insulation resistance test. In those cases where a module failed one of these tests, the cause of the failure was determined.

There are three major outcomes of this outdoor study. First, we have identified several defects in module construction and fabrication that can lead to early field failures. These defects include pinholes in the encapsulant, mechanical damage to the insulation during assembly and defects in assembly techniques. Having identified these defects and how they appear in the fabrication process, we can take steps to eliminate these defects by changing the fabrication steps or installing additional controls, as appropriate. Second, we have clearly established that for certain applications, some of the materials we have tested show clear advantages over other materials. For example, the acrylic urethane materials tested to date have proven to be superior encapsulants when compared to the polyester urethane materials tested to date. Third, for some other applications, we have identified more than one material or method that appear suitable for photovoltaic applications. In these cases, the choice of material or method can be made according to other criteria such as cost or ease of manufacture.

FACTOR	DESCRIPTION
A	Glass Seam Type
B	Contact Metal Type
C	Scribe Type
D	Encapsulation Type
E	Potting Material
F	Connector Design
G	Edge Seal
H	Polarity
I	Mounting Configuration

Table 8.1 The module fabrication and environmental factors investigated in an outdoor exposure study.

RUN	A	B	C	D	E	F	G	H
1	+	+	+	+	+	+	+	+
2	-	-	+	+	+	-	+	-
3	-	-	+	-	-	+	+	+
4	+	+	+	-	-	-	+	-
5	+	-	+	+	-	-	-	+
6	-	+	+	+	-	+	-	-
7	-	+	+	-	+	-	-	+
8	+	-	+	-	+	+	-	-
9	-	+	-	+	-	-	+	+
10	+	-	-	+	-	+	+	-
11	+	-	-	-	+	-	+	+
12	-	+	-	-	+	+	+	-
13	-	-	-	+	+	+	-	+
14	+	+	-	+	+	-	-	-
15	+	+	-	-	-	+	-	+
16	-	-	-	-	-	-	-	-

Table 8.2 Combinations of the factors listed in **Table 8.1** that were used to build up the modules for outdoor exposure study. The plus and minus signs refer to one of two alternatives for the factors A through H.

8.4 Process Yield

At the present time, most of our large-area module fabrication processes are not fully developed. A number of process improvement efforts are underway and because these efforts involve experimentation, the overall process variation is larger than the variation that would be attained if each of the fabrication processes was fixed. As the separate processes become fixed and as process control is established, the total process variation will decrease to the so called natural process variation.

As part of our process control work, we have tracked the process yields at each of the key module fabrication steps for 0.37 m^2 (4 ft^2) size modules. With this data it is possible to estimate the overall process yield. We have defined the overall process yield to be the product of the cumulative yield at each key process step, the wet high potential test yield, and the electrical performance yield. For each of the key process steps, the yield is the ratio of the number of plates passed onto the next process, to the number of plates received by the process. The cumulative process step yield is the product of the yield at each of the major process steps. Over this period our cumulative process yield was 80.6%. The wet high potential test yield is taken to be 80%, which is the wet high potential test yield we achieved using our multi-coat acrylic encapsulant. Our estimate of electrical performance yield is based upon an analysis of the distribution of performance for the large-area modules we produced in this period. Inspection of this distribution suggests that approximately 23.6% of the modules that were passed through the entire fabrication process were subsequently found to have had defects that significantly impacted the performance of the module. These defects occurred during the process but were not detected at the time the process was performed. On the basis of our inspection of the distribution in module performance, we estimate the electrical performance yield of large-area modules to be 76.4%. Our estimate of overall line yield for this period is therefore 0.806 x 0.80 x 0.764 or 49.3%.

In addition to wet high potential test failures, the major causes for line yield loss are losses due to equipment failure, losses due to experimental trials and process failures. The majority of the losses due to equipment and process failures occurred in the early stages of bringing up the equipment or process. As we gained experience, these losses have been steadily reduced. As the fabrication processes become better defined, the variation in the overall process will decline and the overall line yield will increase.

REPORT DOCUMENTATION PAGE

Form Approved
OMB NO. 0704-0188

1. AGENCY USE ONLY (Leave blank)	2. REPORT DATE	3. REPORT TYPE AND DATES COVERED
	November 1994	Annual Subcontract Report, 17 March 1993-18 March 1994

4. TITLE AND SUBTITLE

Large-Area Triple-Junction a-Si Alloy Production Scaleup

5. FUNDING NUMBERS

C: ZM-2-11040-2

TA: PV550101

6. AUTHOR(S)

R. Oswald, J. Morris

7. PERFORMING ORGANIZATION NAME(S) AND ADDRESS(ES)

Solarex Thin-Film Division
826 Newtown-Yardley Road
Newtonw, PA 18940

8. PERFORMING ORGANIZATION REPORT NUMBER

9. SPONSORING/MONITORING AGENCY NAME(S) AND ADDRESS(ES)

National Renewable Energy Laboratory
1617 Cole Blvd.
Golden, CO 80401-3393

10. SPONSORING/MONITORING AGENCY REPORT NUMBER

TP-411-7350

DE95000245

11. SUPPLEMENTARY NOTES

NREL Technical Monitor: R. Mitchell

12a. DISTRIBUTION/AVAILABILITY STATEMENT

12b. DISTRIBUTION CODE

UC-1280

13. ABSTRACT *(Maximum 200 words)*

This report describes work to advance Solarex's photovoltaic manufacturing technologies, reduce its amorphous silicon (a-Si:H) module production costs, increase module performance, and expand the Solarex commercial production capacity. In work reported herein, Solarex focused on improving deposition of the front contact, investigating alternate feedstocks for the front contact, maximizing throughput and area utilization for all laser scribes, optimizing a-Si:H deposition equipment to achieve uniform deposition over large areas, optimizing the triple-junction module fabrication process, evaluating the materials to deposit the rear contact, and optimizing the combination of isolation scribe and encapsulant to pass the wet high potential test.

14. SUBJECT TERMS

manufacturing ; large area ; triple junction ; amorphous silicon ; photovoltaics ; solar cells

15. NUMBER OF PAGES
67

16. PRICE CODE

17. SECURITY CLASSIFICATION OF REPORT	18. SECURITY CLASSIFICATION OF THIS PAGE	19. SECURITY CLASSIFICATION OF ABSTRACT	20. LIMITATION OF ABSTRACT
Unclassified	Unclassified	Unclassified	UL